Engineered Science
DOI: https://dx.doi.org/10.30919/es918

Free and Forced Vibration of Sandwich FGM Porous Variable Thickness Nanoplates Integrated with Magneto-Electro-Elastic Layers Via Nonlocal Strain Gradient Theory

Peyman Roodgar Saffari,[1,*] Sayan Sirimontree,[1] Chanachai Thongchom,[1,*] Thira Jearsiripongkul,[2] Pouyan Roodgar Saffari,[1] Suraparb Keawsawasvong[1] and Suphanut Kongwat[3, 4]

Abstract

In the present study, free and forced vibration analysis of sandwich smart magneto-electro-elastic (MEE) nanoplates with functionally graded material porous (FGMP) of linearly or parabolically varying thickness core layer under initial external electric and magnetic potentials is studied using the first-order shear deformation theory (FSDT) and nonlocal strain gradient theory (NSGT). NSGT is perfected with softening and hardening material effects, which can significantly improve the precision of results. Three states of porosity distribution patterns, *i.e.*, even, uneven, and logarithmic-uneven porosity distributions are considered for the FGMP core layer, which are supposed to vary along the in-plane and thickness directions. The related governing equations are obtained in the time domain by applying Hamilton's principle. The established solution is examined in terms of its precision via a comparison with other available data. Studies of the parameters show the effects of the unidirectional and bidirectional taper constants, initial electric and magnetic potentials, porosity distributions, FG index, nonlocal and strain gradient characteristics on the free and forced vibration.

Keywords: Variable Thickness; Porosity; Free and forced vibration; Magneto-electro-elastic Plate; Nonlocal strain gradient theory.
Received: 27 March 2023; Revised: 25 June 2023; Accepted: 30 June 2023.
Article type: Research article.

1. Introduction

In order to minimize weight while retaining structural integrity, plates of variable thickness are frequently employed in the aerospace industry. It is common practice for aircraft designers to employ a range of thicknesses for the wings and fuselage in order to achieve the best possible strength-to-weight ratio, aerodynamic performance, and fuel efficiency.[1–3] The dynamic response of plates with varying thicknesses has been studied using numerical and analytical techniques. Thi[4] used finite element modelling in temperature conditions to analyze the free vibration behaviors of plates with various thicknesses resting on two-parameter elastic foundations. Ahlawat and Saini[5] examined the influence of thickness variation on the bilaterally symmetrical vibrations of unidirectional circular plates exposed to homogeneous in-plane peripheral loading.

The notion of porosity has been presented in other scientific domains, leading to interesting ideas such as metal foams, which have a number of benefits including greater energy absorption[6,7] and resistance to heat and impact.[8,9] The behavior of porous materials is influenced by the size and porosity of the pores, as well as their shape, arrangement, and surface roughness. To employ such materials in various applications or investigations, it is necessary to describe the relationship between pore characteristics and the physical behavior of such materials. Numerous computational and experimental efforts have examined the effect of porous materials on dynamic aspects, including the free and forced vibration of beams,[10,11] plates[12,13] and cylindrical shells.[14] Plates with high stiffness-to-weight ratios and high strength-

[1] *Department of Civil Engineering, Thammasat School of Engineering, Faculty of Engineering, Thammasat University, Pathumthani 12121, Thailand.*
[2] *Department of Mechanical Engineering, Thammasat School of Engineering, Faculty of Engineering, Thammasat University, Pathumthani 12121, Thailand.*
[3] *Department of Mechanical Engineering, Faculty of Engineering, King Mongkut's University of Technology Thonburi, Bangkok, Thailand, 10140.*
[4] *Future Automotive Structure Research Group (FASt), Mobility and Vehicle Technology Research Center, King Mongkut's University of Technology Thonburi, Bangkok, Thailand, 10140.*
**Email:* peyman.saffari1364@gmail.com (P. R. Saffari); Tchanach@engr.tu.ac.th (C. Thongchom)

to-weight ratios are used in many technical applications, such as airplanes, buildings, submarines, and cars.[15–18] Xue *et al*.[19] investigated the natural frequencies of square, circular, and rectangle porous plates with porosity distributions in the thickness. Using isogeometric analysis (IGA) and FSDT, Gughari *et al*.[20] studied the effects of mechanical/electrical boundary conditions and porosity on the buckling of moderately thick, porous sector and annular sector plates integrated with piezoelectric layers.

In comparison with homogeneous materials, functionally graded materials (FGMs) offer superior performance by combining the required characteristics of each constituent phase.[21–29] Sundararajan *et al*.[30] presented the nonlinear free vibration of FGM rectangular and skew plates subjected to the thermal environment using von Karman's assumptions. Based on the FSDT and Galerkin-Vlasov's method, Kumar *et al*.[31] presented free vibration of a tapered FGMP plate resting on Pasternak substrate applying simple power-law, exponential law, and Sigmoid law. Tahir *et al*.[32] developed a simple integral hyperbolic higher-order shear deformation theory (HSDT) to analyze the wave propagation in an FGM rectangular plate with different porosity distributions. Sah and Ghosh[33] caried out the buckling and free vibration of multi-directional porous FGM sandwich plates. Huang *et al*.[34] used the nonlinear free and forced vibrations of FGMP rectangular plates, taking into account the higher-order shear deformation plate theory and the general von Kármán-type equation.

To analyze the behavior of nanostructures, one can take advantage of two relatively different approaches. When the scale of the analyzed system reduces, an atomistic technique is often infamous for its laborious and time-consuming computations. However, a continuum-based strategy can address the computing issues presented by an atomistic technique.[35–38] Although classical continuum theory can adequately describe the mechanical behavior of materials at the macroscale, it fails spectacularly at the nano- and micro-dimensional levels. The lack of this quality results from the fact that the size dependency of the elastic solutions of an inhomogeneity or inclusion is not well studied. Accordingly, there have been a growing number of theories to deal with size effects at smaller scales. For this reason, a brand-new category of such theories, size-dependent concepts, has been constructed. These recently created notions include strain gradient theory,[39] couple stress theory,[40] and Eringen nonlocal theory.[41] Demir *et al*.[42] utilized the finite element method to examine Eringen's nonlocal elasticity theory for the static behavior of nano-beams under a uniform load and a Winkler substrate. Taking into account the size-dependent behavior and Timoshenko's beam theory in conjunction with nonlocal elasticity theory, Numanoğlu *et al*.[43] developed a study of thermo-mechanical vibrations in nanobeams. The strain energy may be described in terms of length scales, strain gradients, and the strain itself using strain gradient theory (SGT). Additionally, models and experiments revealed that two scale parameters provide the most accurate representation of the mechanical characteristics of nanostructures. As a result, the impacts of stiffness-hardening and stiffness-softening on a nanostructure's mechanics are defined. The nonlocal strain gradient theory (NSGT), which accurately accounts for the influence of the two length scale factors on the physical and mechanical behaviors of size-dependent structures, was proposed by Lim *et al*.[44] by combining the strain gradient and nonlocal elasticity theories. Li and Hu[45] detailed the NSGT-based study of nonlinear bending and free vibration behaviors of functionally graded (FG) beams by deriving and analysing size-dependent nonlinear Euler-Bernoulli and Timoshenko beam models. It has been demonstrated that the stiffness of a FG beam can display either a hardening or softening effect contingent upon the comparative values of the nonlocal and material characteristic parameters. Sobhy *et al*.[46] studied the effect of small scale on the elastic instability and free vibration of double-porous FG nanoplates utilizing new quasi-3D refined plate theory in conjunction with NSGT. According to the NSGT and four-variable plate model, Barati and Shahverdi[47,48] presented forced vibration analysis of heterogeneous porous nanoplates under uniform dynamic load. Ejabati and Fallah[49] developed and presented a size dependent model based on Mindlin's plate and Eringen's non-local theories to analyze the aerodynamic analysis of temperature-dependent FGM nanoplates under a moving nanoparticle. An isogeometric model is used by Thai *et al*.[50] to present the effects of the strain gradient and nonlocal parameters on the natural frequency of the MEE-FG nanoplates via NSGT and higher-order shear deformation theory. Rajput and Gupta[51] studied the effect of geometric imperfections on the thermomechanical nonlinear stability of porous FG nanoplates. For this purpose, they combined the nonlocal strain gradient theory with the inverse trigonometric shear deformation theory. Jiang *et al*.[52] addressed the significance of nonlocal and microstructure-dependent strain gradient effects in polymeric solids when the length scale of external stimulations is comparable to most chain lengths within the material. The findings of this research have implications for understanding the relationship between microstructure-dependent intrinsic lengths and the properties or responses of crosslinked polymer network structures. The physically-based NSGT can contribute to elucidating the influence of microstructural characteristics on the behavior and mechanical properties of polymer networks.

One of the primary reasons so many different types of research have been done on "smart" materials like piezoelectric (PZT), MEE, and electrorheological fluid (ERF) is because of their ability to adapt their properties in response to electricity, magnetic fields, heat, and even mechanical loading.[53–56] With their combined piezoelectric and piezomagnetism properties, MEE composites are an inspiring example of smart composite materials. The capability of transferring energy between various phases explains in part why researchers are interested in these materials.[57–59] A finite element technique (FEM) was given by Vinyas and

Kattimani[60] to determine the static characteristics of rectangular FG MEE plates in a thermal environment. Vinyas[61] applied layerwise shear deformation theory to develop a simple velocity feedback control rule for vibration suppression in skew MEE plates using active constrained layer damping (ACLD). Farajpour *et al*.[62] utilized the NSGT in the framework of von Kármán strain relations to calculate the nonlinear frequency shift of MEE nanoplates. Esayas *et al*.[63] studied the geometrically nonlinear free vibration and transient response of FGMP-MEE nanoplates using FSDT and von Karman's nonlinear strain–displacement relations.

Despite increasing interest in various aspects of the free and forced vibration of nanoplates, the authors were unable to locate any studies that addressed the free and forced vibration of sandwich smart MEE nanoplates with FGMP of a linearly or parabolically varying thickness core layer under the influence of a uniform dynamic load using FSDA and NSGT. The goal of this study is to fill this knowledge gap by offering novel insights into the functioning of such structures. These structures find applications in energy harvesting devices, biomedical engineering for tissue engineering, electronics, and microdevices, as well as catalysis and chemical processing. As a result of three distinct porosity patterns (*i.e.*, even, uneven, and logarithmic-uneven porosity distributions), the material's characteristics exhibit significant variation; a power law model is required to adequately represent these differences. Hamilton's principle is used to obtain the coupled governing equations and associated boundary conditions. For various boundary conditions, the dynamic deflections and resonance frequencies are determined using Galerkin's approach.

2. Preliminary formulations

Figure 1 shows the problem schematically. One should note the employed Cartesian coordinates defined for the rectangular sandwich FGMP-MEE ($L_x \times L_y$) nanoplate. Also, a dynamic of a time-harmonic nature, impinges on the top surface of the upper MEE nanoplate. It is supposed that each MEE nanoplate is composed of two identical $BaTiO_3$-$CoFe_2O_4$ piezomagnetic layers with uniform thickness h_m and a FGMP core layer of variable thickness h that differs linearly or parabolically according to its coordinates (x, y) . Furthermore, each MEE nanoplate is subjected to electric $\Phi(x, y, z, t)$ and magnetic $\Psi(x, y, z, t)$ potentials. The core's thinnest point is indicated by h_0.

The following Equation (1) present the FGMP core layer's thickness variations for bidirectional linearly and parabolically varying thickness:

$$h(x,y) = h_0\left(1 + \frac{\alpha x}{L_x} + \frac{\beta y}{L_y}\right),$$

Bidirectional linear thickness variation, (1)

$$h(x,y) = h_0\left(1 + \frac{\alpha x^2}{{L_x}^2} + \frac{\beta y^2}{{L_y}^2}\right),$$

Bidirectional parabolic thickness variation.

2.1 Constitutive relations

The benefits of FSDT include improved accuracy in stress and displacement predictions, better representation of boundary conditions, and computational efficiency, making it a valuable tool in the analysis and design of thin plate structures. The conventional displacement field U, V, W in Cartesian coordinates for sandwich FGMP-MEE nanoplates is used in the form of the following to derive the dynamic equations governing the motion based on the FSDA, which takes into account both rotary inertia and shear deformation in the transverse direction.[64]

$$\begin{aligned} U(x,y,z,t) &= u_0(x,y,t) + z\theta_x(x,y,t), \\ V(x,y,z,t) &= v_0(x,y,t) + z\theta_y(x,y,t), \\ W(x,y,z,t) &= W_0(x,y,t), \end{aligned} \quad (2)$$

in plane the mid-surface deflections along the x and y axes are shown by u_0 and v_0, respectively. Furthermore θ_y and θ_x are the rotations of the middle plane along x and y directions, respectively, and W_0 denotes the lateral plate displacement. The normal $(\varepsilon_{xx}, \varepsilon_{yy})$ and shear $(\gamma_{xz}, \gamma_{yz}, \gamma_{xy})$ strain components of a sandwich FGMP-MEE nanoplate are characterized in terms of the linear strain-displacement relation as follows:

$$\varepsilon_{xx} = \frac{\partial u_0}{\partial x} + z\frac{\partial \theta_x}{\partial x},\ \varepsilon_{yy} = \frac{\partial v_0}{\partial y} + z\frac{\partial \theta_y}{\partial y}, \quad (3)$$

$$\gamma_{xy} = \frac{\partial u_0}{\partial y} + \frac{\partial v_0}{\partial x} + z\left(\frac{\partial \theta_x}{\partial y} + \frac{\partial \theta_y}{\partial x}\right), \gamma_{xz} = \theta_x + \frac{\partial w_0}{\partial x},$$

$$\gamma_{yz} = \theta_y + \frac{\partial w_0}{\partial y}.$$

For the FGMP core layer in a sandwich nanoplate, the nonclassical constitutive stress-strain relations are provided as:[65–67]

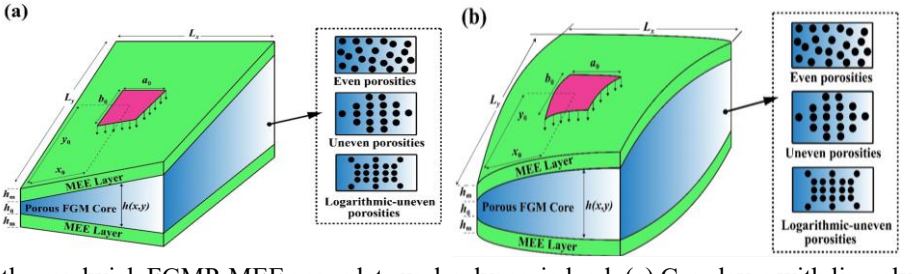

Fig. 1 The schematic of the sandwich FGMP-MEE nanoplate under dynamic load; (a) Core layer with linearly varying thickness; (b) Core layer with parabolically varying thickness.

$$\left[1-(e_0a)^2\left(\frac{\partial^2}{\partial x^2}+\frac{\partial^2}{\partial y^2}\right)\right]\begin{bmatrix}\sigma_{xx}\\ \sigma_{yy}\\ \sigma_{xy}\\ \sigma_{yz}\\ \sigma_{xz}\end{bmatrix}_{\mathrm{FGMP}}=\left[1-l^2\left(\frac{\partial^2}{\partial x^2}+\frac{\partial^2}{\partial y^2}\right)\right]\begin{bmatrix}Q_{11}(z) & Q_{12(z)} & 0 & 0 & 0\\ Q_{12(z)} & Q_{22}(z) & 0 & 0 & 0\\ 0 & 0 & Q_{66}(z) & 0 & 0\\ 0 & 0 & 0 & k_sQ_{44}(z) & 0\\ 0 & 0 & 0 & 0 & k_sQ_{55}(z)\end{bmatrix}_{\mathrm{FGMP}}\begin{bmatrix}\varepsilon_{xx}\\ \varepsilon_{yy}\\ \gamma_{xy}\\ \gamma_{yz}\\ \gamma_{xz}\end{bmatrix}$$

$$Q_{11}=\frac{E(x,y,z)}{1-\vartheta^2(x,y,z)},Q_{22}=\frac{E(x,y,z)}{1-\vartheta^2(x,y,z)},$$
$$Q_{12}=\frac{\vartheta(x,y,z)E(x,y,z)}{1-\vartheta^2(x,y,z)},Q_{66}=G_{12}(x,y,z),$$
$$Q_{44}=G_{23}(x,y,z),Q_{55}=G_{13}(x,y,z), \quad (4)$$

where the shear correction component is represented by the symbol $k_s=5/6$. With the help of this correction factor, warping of cross-sections is taken into consideration in the shear deformation and stress calculations. The shear correction factor is normally calculated empirically or numerically, and its value is shape- and size-dependent. Additionally, E and ϑ refer to the Young's modulus and Poisson's ratio of the FGMP core layer, respectively. In addition, the symbols l and e_0a a stand for the strain gradient and nonlocal parameter, respectively. a stands for the internal characteristic length, while e_0 is the calibration constant. Based on previous research, it has been demonstrated that the thickness effect has a considerable impact on the dynamic behavior of nanoscale structures. Therefore, it is necessary to consider the high order nonlocal stresses in the NSGT. To better understand this matter, readers are encouraged to refer to Ref. [68]. To get FG-like properties, the bottom layer of the core is made of metal and the top layer is made of ceramic. Three porosity distribution patterns are taken into consideration for this investigation, as already mentioned. The values of elastic modulus, mass density, and Poisson's ratio are given in accordance with the law of mixing as:[69]

Even porosity dispersion:

$$E(x,y,z)=(E_{\mathrm{c}}-E_{\mathrm{m}})(z/h(x,y)+0.5)^p+E_{\mathrm{m}}-0.5\zeta(E_{\mathrm{c}}+E_{\mathrm{m}}),$$
$$\rho(x,y,z)=(\rho_{\mathrm{c}}-\rho_{\mathrm{m}})(z/h(x,y)+0.5)^p+\rho_{\mathrm{m}}-0.5\zeta(\rho_{\mathrm{c}}+\rho_{\mathrm{m}}), \quad (5)$$
$$\vartheta(x,y,z)=(\vartheta_{\mathrm{c}}-\vartheta_{\mathrm{m}})(z/h(x,y)+0.5)^p+\vartheta_{\mathrm{m}}-0.5\zeta(\vartheta_{\mathrm{c}}+\vartheta_{\mathrm{m}}),$$

Uneven porosity dispersion:

$$E(x,y,z)=(E_{\mathrm{c}}-E_{\mathrm{m}})(z/h(x,y)+0.5)^p+E_{\mathrm{m}}-0.5\zeta(E_{\mathrm{c}}+E_{\mathrm{m}})(1-2|z|/h(x,y)),$$
$$\rho(x,y,z)=(\rho_{\mathrm{c}}-\rho_{\mathrm{m}})(z/h(x,y)+0.5)^p+\rho_{\mathrm{m}}-0.5\zeta(\rho_{\mathrm{c}}+\rho_{\mathrm{m}})(1-2|z|/h(x,y)), \quad (6)$$
$$\vartheta(x,y,z)=(\vartheta_{\mathrm{c}}-\vartheta_{\mathrm{m}})(z/h(x,y)+0.5)^p+\vartheta_{\mathrm{m}}-0.5\zeta(\vartheta_{\mathrm{c}}+\vartheta_{\mathrm{m}})(1-2|z|/h(x,y)),$$

Logarithmic uneven porosity dispersion

$$E(x,y,z)=(E_{\mathrm{c}}-E_{\mathrm{m}})(z/h(x,y)+0.5)^p+E_{\mathrm{m}}-\log(1+0.5\zeta)(E_{\mathrm{c}}+E_{\mathrm{m}})(1-2|z|/h(x,y)),$$
$$\rho(x,y,z)=(\rho_{\mathrm{c}}-\rho_{\mathrm{m}})(z/h(x,y)+0.5)^p+\rho_{\mathrm{m}}-\log(1+0.5\zeta)(\rho_{\mathrm{c}}+\rho_{\mathrm{m}})(1-2|z|/h(x,y)), \quad (7)$$
$$\vartheta(x,y,z)=(\vartheta_{\mathrm{c}}-\vartheta_{\mathrm{m}})(z/h(x,y)+0.5)^p+\vartheta_{\mathrm{m}}-\log(1+0.5\zeta)(\vartheta_{\mathrm{c}}+\vartheta_{\mathrm{m}})(1-2|z|/h(x,y)),$$

where the symbols for the metal and ceramic phases, respectively, are m and c. Furthermore, ρ stands for mass density as well. The gradient index (p), which is always positive, is used to describe how a specific property changes in the thickness direction. Increases in the gradient index indicate a more metallic structure. Additionally, ζ represents the porosity coefficient. It is worth noting that, according to the NSGT, the essential relationships for MEE nanoplates, including electric displacement, magnetic induction, and stress tensor, may be written as:[70,71]

$$\left[1-(e_0a)^2\left(\frac{\partial^2}{\partial x^2}+\frac{\partial^2}{\partial y^2}\right)\right]\begin{bmatrix}\sigma_{xx}\\ \sigma_{yy}\\ \sigma_{yz}\\ \sigma_{xz}\\ \sigma_{xy}\end{bmatrix}_{\mathrm{MEE}}=\left[1-l^2\left(\frac{\partial^2}{\partial x^2}+\frac{\partial^2}{\partial y^2}\right)\right]\left(\begin{bmatrix}\underline{C}_{11} & \underline{C}_{12} & 0 & 0 & 0\\ \underline{C}_{21} & \underline{C}_{22} & 0 & 0 & 0\\ 0 & 0 & k_s\underline{C}_{44} & 0 & 0\\ 0 & 0 & 0 & k_s\underline{C}_{44} & 0\\ 0 & 0 & 0 & 0 & \underline{C}_{66}\end{bmatrix}\begin{Bmatrix}\varepsilon_{xx}\\ \varepsilon_{yy}\\ \gamma_{yz}\\ \gamma_{xz}\\ \gamma_{xy}\end{Bmatrix}-\begin{bmatrix}0 & 0 & \underline{e}_{31}\\ 0 & 0 & \underline{e}_{31}\\ 0 & \underline{e}_{24} & 0\\ \underline{e}_{15} & 0 & 0\\ 0 & 0 & 0\end{bmatrix}\begin{Bmatrix}\mathbb{E}_x\\ \mathbb{E}_y\\ \mathbb{E}_z\end{Bmatrix}-\begin{bmatrix}0 & 0 & \underline{q}_{31}\\ 0 & 0 & \underline{q}_{31}\\ 0 & \underline{q}_{24} & 0\\ \underline{q}_{24} & 0 & 0\\ 0 & 0 & 0\end{bmatrix}\begin{Bmatrix}\mathbb{H}_x\\ \mathbb{H}_y\\ \mathbb{H}_z\end{Bmatrix}\right),$$

$$\left[1-(e_0a)^2\left(\frac{\partial^2}{\partial x^2}+\frac{\partial^2}{\partial y^2}\right)\right]\begin{bmatrix}\mathfrak{D}_x\\ \mathfrak{D}_y\\ \mathfrak{D}_z\end{bmatrix}=\left[1-l^2\left(\frac{\partial^2}{\partial x^2}+\frac{\partial^2}{\partial y^2}\right)\right]\left(\begin{bmatrix}0 & 0 & 0 & \underline{e}_{15} & 0\\ 0 & 0 & \underline{e}_{24} & 0 & 0\\ \underline{e}_{31} & \underline{e}_{31} & 0 & 0 & 0\end{bmatrix}\begin{Bmatrix}\varepsilon_{xx}\\ \varepsilon_{yy}\\ \gamma_{yz}\\ \gamma_{xz}\\ \gamma_{xy}\end{Bmatrix}+\begin{bmatrix}\underline{k}_{11} & 0 & 0\\ 0 & \underline{k}_{22} & 0\\ 0 & 0 & \underline{k}_{33}\end{bmatrix}\begin{Bmatrix}\mathbb{E}_x\\ \mathbb{E}_y\\ \mathbb{E}_z\end{Bmatrix}+\begin{bmatrix}\underline{a}_{11} & 0 & 0\\ 0 & \underline{a}_{22} & 0\\ 0 & 0 & \underline{a}_{33}\end{bmatrix}\begin{Bmatrix}\mathbb{H}_x\\ \mathbb{H}_y\\ \mathbb{H}_z\end{Bmatrix}\right),$$

$$\left[1-(e_0a)^2\left(\frac{\partial^2}{\partial x^2}+\frac{\partial^2}{\partial y^2}\right)\right]\begin{bmatrix}\mathfrak{B}_x\\ \mathfrak{B}_y\\ \mathfrak{B}_z\end{bmatrix}=\left[1-l^2\left(\frac{\partial^2}{\partial x^2}+\frac{\partial^2}{\partial y^2}\right)\right]\left(\begin{bmatrix}0 & 0 & 0 & \underline{q}_{15} & 0\\ 0 & 0 & \underline{q}_{24} & 0 & 0\\ \underline{q}_{31} & \underline{q}_{31} & 0 & 0 & 0\end{bmatrix}\begin{Bmatrix}\varepsilon_{xx}\\ \varepsilon_{yy}\\ \gamma_{yz}\\ \gamma_{xz}\\ \gamma_{xy}\end{Bmatrix}+\right.$$

$$\left.\begin{bmatrix} \underline{a}_{11} & 0 & 0 \\ 0 & \underline{a}_{22} & 0 \\ 0 & 0 & \underline{a}_{33} \end{bmatrix}\begin{Bmatrix} \mathbb{E}_x \\ \mathbb{E}_y \\ \mathbb{E}_z \end{Bmatrix} + \begin{bmatrix} \underline{\mu}_{11} & 0 & 0 \\ 0 & \underline{\mu}_{22} & 0 \\ 0 & 0 & \underline{\mu}_{33} \end{bmatrix}\begin{Bmatrix} \mathbb{H}_x \\ \mathbb{H}_y \\ \mathbb{H}_z \end{Bmatrix}\right). \quad (8)$$

where $[\mathfrak{B}]$ denotes magnetic induction and $[\mathfrak{D}]$ denotes electric displacement. Also, the elastic constant matrix $\left[\underline{C}\right]$, the magnetic constant matrix $\left[\underline{\mu}\right]$, the magnetoelectric constant matrix $\left[\underline{a}\right]$, the dielectric constant matrix $\left[\underline{k}\right]$, the piezoelectric constant matrix $\left[\underline{q}\right]$, and the piezomagnetic constant matrix $\left[\underline{e}\right]$ can be shown as:

$$\underline{C}_{11} = C_{11} - \frac{{C_{13}}^2}{C_{33}},\ \bar{C}_{12} = C_{12} - \frac{C_{13}C_{23}}{C_{33}},$$
$$\underline{C}_{22} = C_{22} - \frac{{C_{23}}^2}{C_{33}}, \underline{C}_{44} = C_{44},\ \underline{C}_{55} = C_{55},$$
$$\underline{C}_{66} = C_{66},\ \underline{e}_{31} = e_{31} - \frac{C_{13}e_{33}}{C_{33}}, \underline{e}_{32} = e_{32} - \frac{C_{23}e_{33}}{C_{33}},$$
$$\underline{e}_{24} = e_{24},\ \underline{e}_{15} = e_{15},\ \underline{q}_{31} = q_{31} - \frac{C_{13}q_{33}}{C_{33}},$$
$$\underline{q}_{32} = q_{32} - \frac{C_{23}q_{33}}{C_{33}}, \underline{q}_{24} = q_{24}, \underline{q}_{15} = q_{15},$$
$$\underline{k}_{11} = K_{11},\ \underline{k}_{22} = k_{11}, \underline{k}_{33} = k_{33} + \frac{{e_{33}}^2}{C_{33}}, \underline{a}_{11} = a_{11},$$
$$\underline{a}_{22} = a_{22},\ \underline{a}_{33} = a_{33} + \frac{q_{33}e_{33}}{C_{33}}, \underline{\mu}_{11} = \mu_{11}, \underline{\mu}_{22} = \mu_{22},$$
$$\underline{\mu}_{33} = \mu_{33} + \frac{{q_{33}}^2}{C_{33}}. \quad (9)$$

$[\mathbb{H}]$ and $[\mathbb{E}]$ show the magnetic and electric fields related to the magnetic and electric potentials, respectively. In order to meet Maxwell's equations, the magnetic field is assumed to be the negative gradient of $\psi(x, y, z, t)$, and the electric field is assumed to be the negative gradient of $\Phi(x, y, z, t)$.

$$\mathbb{E}_j = -\partial\Phi/\partial j,\ \mathbb{H}_j = -\partial\Psi/\partial j,\ \ (j = x, y, z). \quad (10)$$

It is conceivable to use a combination of linear and cosine variations to clearly define the electric and magnetic potentials in light of the boundary conditions at the top and bottom surfaces of each MEE layer.[72]

$$\Phi(x,y,z,t) = -\cos\left\{\frac{\pi\left[z \pm \left(\frac{h(x,y)+h_{\mathrm{m}}}{2}\right)\right]}{h_{\mathrm{m}}}\right\}\phi(x,y,t) + \frac{2\left[z \pm \left(\frac{h(x,y)+h_{\mathrm{m}}}{2}\right)\right]\phi_0}{h_{\mathrm{m}}},$$

$$\Psi(x,y,z,t) = -\cos\left\{\frac{\pi\left[z \pm \left(\frac{h(x,y)+h_{\mathrm{m}}}{2}\right)\right]}{h_{\mathrm{m}}}\right\}\psi(x,y,t) + \frac{2\left[z \pm \left(\frac{h(x,y)+h_{\mathrm{m}}}{2}\right)\right]\psi_0}{h_{\mathrm{m}}}, \quad (11)$$

where, on the upper and bottom surfaces of each MEE layer, respectively, ϕ_0 and ψ_0 signify the initial electric and magnetic potentials. Additionally, ϕ and ψ stand for the two-dimensional electric and magnetic potentials. In order to get the equilibrium equations of motion, Hamilton's principle is used as:[73,74]

$$\int_0^t \delta\left(\Pi_s + \Pi_f - \Pi_K\right) dt = 0, \quad (12)$$

where $\delta\Pi_{\mathrm{K}}, \delta\Pi_{\mathrm{f}}, \delta\Pi_{\mathrm{s}}$ represent variations in kinetic energy, external force work (harmonic load work), and strain energy, respectively. For a sandwich FGMP-MEE nanoplate, the kinetic energy variation is represented as:

$$\Pi_K = \iint_A \left[I_0\left(\dot{u}_0\delta\dot{u}_0 + \dot{V}_0\delta\dot{V}_0 + \dot{W}_0\delta\dot{W}_0\right) + I_1\left(\dot{u}_0\delta\dot{\theta}_x + \dot{V}_0\delta\dot{\theta}_y + \dot{\theta}_x\delta\dot{u}_0 + \dot{\theta}_y\delta\dot{V}_0\right)\right. \quad (13)$$

where A is the of cross-sectional area, and

$$I_0 = \int_{-h_{\mathrm{m}}-h(x,y)/2}^{-h(x,y)/2}\rho_{\mathrm{m}}dz + \int_{-h(x,y)/2}^{h(x,y)/2}\rho(z)dz + \int_{h(x,y)/2}^{h(x,y)/2+h_{\mathrm{m}}}\rho_{\mathrm{m}}dz,$$
$$I_1 = \int_{-h_{\mathrm{m}}-h(x,y)/2}^{-h(x,y)/2}\rho_{\mathrm{m}}zdz + \int_{-h(x,y)/2}^{h(x,y)/2}\rho(z)zdz + \int_{h(x,y)/2}^{h(x,y)/2+h_{\mathrm{m}}}\rho_{\mathrm{m}}zdz\,,$$
$$I_2 = \int_{-h_{\mathrm{m}}-h(x,y)/2}^{-h(x,y)/2}\rho_{\mathrm{m}}z^2dz + \int_{-h(x,y)/2}^{h(x,y)/2}\rho(z)z^2dz + \int_{h(x,y)/2}^{h(x,y)/2+h_{\mathrm{m}}}\rho_{\mathrm{m}}z^2dz\,, \quad (14)$$

The variation of strain energy is shown as:

$$\delta\Pi_s = \int\int_{-h_{\mathrm{m}}-h(x,y)/2}^{-h(x,y)/2}\left(\sigma_{xx}^{\mathrm{MEE}}\delta\varepsilon_{xx} + \sigma_{yy}^{\mathrm{MEE}}\delta\varepsilon_{yy} + \sigma_{xy}^{\mathrm{MEE}}\delta\gamma_{xy} + \sigma_{xz}^{\mathrm{MEE}}\delta\gamma_{xz} + \sigma_{yz}^{\mathrm{MEE}}\delta\gamma_{yz} - \mathfrak{D}_{xB}\mathbb{E}_{xB} - \mathfrak{D}_{yB}\mathbb{E}_{yB} - \mathfrak{D}_{zB}\mathbb{E}_{zB} - \mathfrak{B}_{xB}\mathbb{H}_{xB} - \mathfrak{B}_{yB}\mathbb{H}_{yB} - \mathfrak{B}_{zB}\mathbb{H}_{zB}\right)dzdA + \int\int_{-h(x,y)/2}^{h(x,y)/2}\left(\sigma_{xx}^{\mathrm{FGMP}}\delta\varepsilon_{xx} + \sigma_{yy}^{\mathrm{FGMP}}\delta\varepsilon_{yy} + \sigma_{xy}^{\mathrm{FGMP}}\delta\gamma_{xy} + \sigma_{xz}^{\mathrm{FGMP}}\delta\gamma_{xz} + \sigma_{yz}^{\mathrm{FGMP}}\delta\gamma_{yz}\right)dzdA + \int\int_{h(x,y)/2}^{h(x,y)/2+h_{\mathrm{m}}}\left(\sigma_{xx}^{\mathrm{MEE}}\delta\varepsilon_{xx} + \sigma_{yy}^{\mathrm{MEE}}\delta\varepsilon_{yy} + \sigma_{xy}^{\mathrm{MEE}}\delta\gamma_{xy} + \sigma_{xz}^{\mathrm{MEE}}\delta\gamma_{xz} + \sigma_{yz}^{\mathrm{MEE}}\delta\gamma_{yz} - \mathfrak{D}_{xT}\mathbb{E}_{xT} - \mathfrak{D}_{yT}\mathbb{E}_{yT} - \mathfrak{D}_{zT}\mathbb{E}_{zT} - \mathfrak{B}_{xT}\mathbb{H}_{xT} - \mathfrak{B}_{yT}\mathbb{H}_{yT} - \mathfrak{B}_{zT}\mathbb{H}_{zT}\right)dzdA =$$
$$\int\int_{-h_{\mathrm{m}}-h(x,y)/2}^{-h(x,y)/2}\left(\sigma_{xx}^{\mathrm{MEE}}\delta\left[\frac{\partial u_0}{\partial x} + z\frac{\partial\theta_x}{\partial x}\right] + \sigma_{yy}^{\mathrm{MEE}}\delta\left[\frac{\partial v_0}{\partial y} + z\frac{\partial\theta_y}{\partial y}\right] + \sigma_{xy}^{\mathrm{MEE}}\delta\left[\frac{\partial u_0}{\partial y} + \frac{\partial v_0}{\partial x} + z\left(\frac{\partial\theta_x}{\partial y} + \frac{\partial\theta_y}{\partial x}\right)\right] + \sigma_{xz}^{\mathrm{MEE}}\delta\left[\theta_x + \frac{\partial w_0}{\partial x}\right] + \sigma_{yz}^{\mathrm{MEE}}\delta\left[\theta_y + \frac{\partial w_0}{\partial y}\right] - \mathfrak{D}_{xB}\mathbb{E}_{xB} - \mathfrak{D}_{yB}\mathbb{E}_{yB} - \mathfrak{D}_{zB}\mathbb{E}_{zB} - \mathfrak{B}_{xB}\mathbb{H}_{xB} - \mathfrak{B}_{yB}\mathbb{H}_{yB} - \mathfrak{B}_{zB}\mathbb{H}_{zB}\right)dzdA +$$
$$\int\int_{-h(x,y)/2}^{h(x,y)/2}\left(\sigma_{xx}^{\mathrm{FGMP}}\delta\left[\frac{\partial u_0}{\partial x} + z\frac{\partial\theta_x}{\partial x}\right] + \sigma_{yy}^{\mathrm{FGMP}}\delta\left[\frac{\partial v_0}{\partial y} + z\frac{\partial\theta_y}{\partial y}\right] + \sigma_{xy}^{\mathrm{FGMP}}\delta\left[\frac{\partial u_0}{\partial y} + \frac{\partial v_0}{\partial x} + z\left(\frac{\partial\theta_x}{\partial y} + \frac{\partial\theta_y}{\partial x}\right)\right] + \sigma_{xz}^{\mathrm{FGMP}}\delta\left[\theta_x + \frac{\partial w_0}{\partial x}\right] + \sigma_{yz}^{\mathrm{FGMP}}\delta\left[\theta_y + \frac{\partial w_0}{\partial y}\right]\right)dzdA + \int\int_{h(x,y)/2}^{h(x,y)/2+h_{\mathrm{m}}}\left(\sigma_{xx}^{\mathrm{MEE}}\delta\left[\frac{\partial u_0}{\partial x} + z\frac{\partial\theta_x}{\partial x}\right] + \sigma_{yy}^{\mathrm{MEE}}\delta\left[\frac{\partial v_0}{\partial y} + z\frac{\partial\theta_y}{\partial y}\right] + \sigma_{xy}^{\mathrm{MEE}}\delta\left[\frac{\partial u_0}{\partial y} + \frac{\partial v_0}{\partial x} + z\left(\frac{\partial\theta_x}{\partial y} + \frac{\partial\theta_y}{\partial x}\right)\right] + \sigma_{xz}^{\mathrm{MEE}}\delta\left[\theta_x + \frac{\partial w_0}{\partial x}\right] + \sigma_{yz}^{\mathrm{MEE}}\delta\left[\theta_y + \frac{\partial w_0}{\partial y}\right] - \mathfrak{D}_{xT}\mathbb{E}_{xT} - \mathfrak{D}_{yT}\mathbb{E}_{yT} - \mathfrak{D}_{zT}\mathbb{E}_{zT} - \mathfrak{B}_{xT}\mathbb{H}_{xT} - \mathfrak{B}_{yT}\mathbb{H}_{yT} - \mathfrak{B}_{zT}\mathbb{H}_{zT}\right)dzdA\,. \quad (15)$$

The variation in work caused by external forces is defined as:

$$\delta\Pi_f = \int_A \left\{q_{DYN}\delta W_0 + (N_E + N_M)\delta\left[\left(\frac{\partial W_0}{\partial x}\right)^2 + \left(\frac{\partial W_0}{\partial y}\right)^2\right]\right\}\mathrm{d}A\,. \quad (16)$$

in which $N_M = \int_{-h_m-h(x,y)/2}^{-h(x,y)/2} 2\,f_{31}\psi_0/h_m dz + \int_{h(x,y)/2}^{h_m+h(x,y)/2} 2\,f_{31}\,\psi_0/h_m dz$ and $N_E = \int_{-h_m-h(x,y)/2}^{-h(x,y)/2} 2\,e_{31}\,\phi_0/h_m dz + \int_{h(x,y)/2}^{h_m+h(x,y)/2} 2\,e_{31}\,\phi_0/h_m dz$. To get the governing equations of motion, we insert Equations (13), (15), and (16) into Equation (12) as:

$$\delta u_0 \to \frac{\partial N_{xx}}{\partial x} + \frac{\partial N_{xy}}{\partial y} = I_0\ddot{u_0} + I_1\ddot{\theta_x},$$
$$\delta v_0 \to \frac{\partial N_{yy}}{\partial y} + \frac{\partial N_{xy}}{\partial x} = I_0\ddot{v_0} + I_1\ddot{\theta}_y\,,$$
$$\delta W_0 \to \frac{\partial Q_{xz}}{\partial x} + \frac{\partial Q_{yz}}{\partial y} = q_{DYN} + I_0\ddot{W_0} - N_E\left(\frac{\partial^2 W_0}{\partial x^2} + \frac{\partial^2 W_0}{\partial y^2}\right) - N_M\left(\frac{\partial^2 W_0}{\partial x^2} + \frac{\partial^2 W_0}{\partial y^2}\right),$$
$$\delta\theta_x \to \frac{\partial M_{xx}}{\partial x} + \frac{\partial M_{xy}}{\partial y} - Q_{xz} = I_1\ddot{u_0} + I_2\ddot{\theta_x}\,,$$
$$\delta\theta_y \to \frac{\partial M_{yy}}{\partial y} + \frac{\partial M_{xy}}{\partial x} - Q_{yz} = I_1\ddot{v_0} + \bar{I}_2\ddot{\theta}_y, \qquad (17)$$

in which the resultant momentum $N_{ij}, M_{ij}, P_{ij}, Q_{ij}, R_{ij}$ are represented as

$$(N_{xx}, M_{xx}) = \int_{-h_m-\frac{h(x,y)}{2}}^{-\frac{h(x,y)}{2}} \sigma_{xx}^{\mathrm{MEE}}(1,z)dz + \int_{-\frac{h(x,y)}{2}}^{\frac{h(x,y)}{2}} \sigma_{xx}^{\mathrm{FGMP}}(1,z)dz + \int_{\frac{h(x,y)}{2}}^{\frac{h(x,y)}{2}+h_m} \sigma_{xx}^{\mathrm{MEE}}(1,z)dz,$$
$$(N_{xy}, M_{xy}) = \int_{-h_m-\frac{h(x,y)}{2}}^{-\frac{h(x,y)}{2}} \sigma_{xy}^{\mathrm{MEE}}(1,z)dz + \int_{-\frac{h(x,y)}{2}}^{\frac{h(x,y)}{2}} \sigma_{xy}^{\mathrm{FGMP}}(1,z)dz + \int_{\frac{h(x,y)}{2}}^{\frac{h(x,y)}{2}+h_m} \sigma_{xy}^{\mathrm{MEE}}(1,z)dz,$$
$$(N_{yy}, M_{yy}) = \int_{-h_m-\frac{h(x,y)}{2}}^{-\frac{h(x,y)}{2}} \sigma_{yy}^{\mathrm{MEE}}(1,z)dz + \int_{-\frac{h(x,y)}{2}}^{\frac{h(x,y)}{2}} \sigma_{yy}^{\mathrm{FGMP}}(1,z)dz + \int_{\frac{h(x,y)}{2}}^{\frac{h(x,y)}{2}+h_m} \sigma_{yy}^{\mathrm{MEE}}(1,z)dz,$$
$$Q_{xz} = \int_{-h_m-\frac{h(x,y)}{2}}^{-\frac{h(x,y)}{2}} \sigma_{xz}^{\mathrm{MEE}}dz + \int_{-\frac{h(x,y)}{2}}^{\frac{h(x,y)}{2}} \sigma_{xz}^{\mathrm{FGMP}}dz + \int_{\frac{h(x,y)}{2}}^{\frac{h(x,y)}{2}+h_m} \sigma_{xz}^{\mathrm{MEE}}dz\,, Q_{yz} = \int_{-h_m-\frac{h(x,y)}{2}}^{-\frac{h(x,y)}{2}} \sigma_{yz}^{\mathrm{MEE}}dz + \int_{-\frac{h(x,y)}{2}}^{\frac{h(x,y)}{2}} \sigma_{yz}^{\mathrm{FGMP}}dz + \int_{\frac{h(x,y)}{2}}^{\frac{h(x,y)}{2}+h_m} \sigma_{yz}^{\mathrm{MEE}}dz, \qquad (18)$$

As well, the corresponding boundary conditions can be obtained by considering the variations at the endpoints of the time interval. This involves evaluating the variation of the action functional at the initial and final times based on the Hamilton's variational principle as:

$$\delta u_0 \to N_{xx}n_x + n_yN_{xy} = 0, \qquad (19)$$
$$\delta v_0 \to N_{xy}n_x + N_{yy}n_y = 0,$$
$$\delta W_0 \to \left(n_x\left(Q_{xz} + (N_E + N_M)\frac{\partial W_0}{\partial x}\right) + n_y\left(Q_{yz} + (N_E + N_M)\frac{\partial W_0}{\partial y}\right) = 0\,,$$
$$\delta\theta_x \to n_xM_{xx} + n_yM_{xy} = 0,$$
$$\delta\theta_y \to n_yM_{yy} + n_xM_{xy} = 0,$$
$$\delta\phi \to \int_{-h_m-h(x,y)/2}^{-h(x,y)/2}\left[n_x\mathfrak{D}_{xB}cos\left\langle\frac{\pi\left[z+\left(\frac{h(x,y)+h_m}{2}\right)\right]}{h_m}\right\rangle + n_y\mathfrak{D}_{yB}cos\left\langle\frac{\pi\left[z+\left(\frac{h(x,y)+h_m}{2}\right)\right]}{h_m}\right\rangle\right]dz +$$
$$\int_{h(x,y)/2}^{h(x,y)/2+h_m}\left[n_x\mathfrak{D}_{xT}cos\left\langle\frac{\pi\left[z-\left(\frac{h(x,y)+h_m}{2}\right)\right]}{h_m}\right\rangle + n_y\mathfrak{D}_{yT}cos\left\langle\frac{\pi\left[z-\left(\frac{h(x,y)+h_m}{2}\right)\right]}{h_m}\right\rangle\right]dz = 0\,,$$
$$\delta\psi \to \int_{-h_m-h(x,y)/2}^{-h(x,y)/2}\left[n_x\mathfrak{B}_{xB}cos\left\langle\frac{\pi\left[z+\left(\frac{h(x,y)+h_m}{2}\right)\right]}{h_m}\right\rangle + n_y\mathfrak{B}_{yB}cos\left\langle\frac{\pi\left[z+\left(\frac{h(x,y)+h_m}{2}\right)\right]}{h_m}\right\rangle\right]dz +$$
$$\int_{h(x,y)/2}^{h(x,y)/2+h_m}\left[n_x\mathfrak{B}_{xT}cos\left\langle\frac{\pi\left[z-\left(\frac{h(x,y)+h_m}{2}\right)\right]}{h_m}\right\rangle + n_y\mathfrak{B}_{yT}cos\left\langle\frac{\pi\left[z-\left(\frac{h(x,y)+h_m}{2}\right)\right]}{h_m}\right\rangle\right]dz = 0.$$

In the end, the equilibrium equations for a sandwich FGMP-MEE nanoplate are found by substituting Equation (18) into Equation (17) with respect to Equations (2-4) and (8), which provided in APPENDIX A.

3. Solution method

The boundary conditions of the sandwiched FGMP-MEE nanoplate's four corners should be as follows in order to analytically solve the governing equations of motion (A1-A7) Clamped (C) edge boundary conditions.

$$u_0 = v_0 = W_0 = \theta_x = \theta_y = \phi = \Psi = \theta_y = 0, \quad at\ x = 0, L_x;\ \ y = 0, L_y. \qquad (20)$$

Simply supported (S) edge boundary conditions.

$$v_0 = W_0 = \theta_y = \phi = \Psi = N_{xx} = M_{xx} = P_{xx} = 0, \quad at\ x = 0, L_x,$$
$$u_0 = W_0 = \theta_x = \phi = \Psi = N_{yy} = M_{yy} = P_{yy} = 0, \quad at\ y = 0, L_y. \qquad (21)$$

For the corresponding boundary conditions, the following appropriate formulations are used[75,76]

$$u_0 = \sum_m^\infty\sum_n^\infty \tilde{U}\frac{\partial X_m(x)}{\partial x}Y_n(y)e^{i\omega t}, \qquad (22)$$
$$v_0 = \sum_m^\infty\sum_n^\infty \tilde{V}X_m(x)\frac{\partial Y_n(y)}{\partial y}e^{i\omega t},$$
$$W_0 = \sum_m^\infty\sum_n^\infty \tilde{W}Y_n(y)X_m(x)e^{i\omega t},$$
$$\theta_x = \sum_m^\infty\sum_n^\infty \tilde{\theta}_x\frac{\partial X_m(x)}{\partial x}Y_n(y)e^{i\omega t},$$
$$\theta_y = \sum_m^\infty\sum_n^\infty \tilde{\theta}_yX_m(x)\frac{\partial Y_n(y)}{\partial y}e^{i\omega t},$$
$$\phi = \sum_m^\infty\sum_n^\infty \tilde{\phi}Y_n(y)X_m(x)e^{i\omega t},$$
$$\Psi = \sum_m^\infty\sum_n^\infty \tilde{\Psi}Y_n(y)X_m(x)e^{i\omega t}\,,$$

where ω displays the angular frequency and m and n are, respectively, the half wave numbers along x and y directions. Moreover, $(\tilde{U}, \tilde{V}, \tilde{W}, \tilde{\theta}_x, \tilde{\theta}_y, \tilde{\phi}, \tilde{\Psi})$ represent the unknown modal coefficients associated with the sandwich FGMP-MEE nanoplate and denoted as:[75]

$$X_m(x) = sin\left(\frac{m\pi x}{L_x}\right), \qquad (23)$$
$$Y_n(y) = sin\left(\frac{n\pi y}{L_y}\right)$$

CSCS

$$X_m(x)=\left[sin\left(\frac{(m+0.25)\pi x}{L_x}\right)-sinh\left(\frac{(m+0.25)\pi x}{L_x}\right)\right]-\left[\frac{sin((m+0.25)\pi)+sinh((m+0.25)\pi)}{cos((m+0.25)\pi)+cosh((m+0.25)\pi)}\right]\left[cos\left(\frac{(m+0.25)\pi x}{L_x}\right)-cosh\left(\frac{(m+0.25)\pi x}{L_x}\right)\right],$$

$$Y_n(y)=\left[sin\left(\frac{(n+0.25)\pi y}{L_y}\right)-sinh\left(\frac{(n+0.25)\pi y}{L_y}\right)\right]-\left[\frac{sin((n+0.25)\pi)+sinh((n+0.25)\pi)}{cos((n+0.25)\pi)+cosh((n+0.25)\pi)}\right]\left[cos\left(\frac{(n+0.25)\pi y}{L_y}\right)-cosh\left(\frac{(n+0.25)\pi y}{L_y}\right)\right],\quad \text{CCCC} \tag{24}$$

$$X_m(x)=\left[sin\left(\frac{(m+0.5)\pi x}{L_x}\right)-sinh\left(\frac{(m+0.5)\pi x}{L_x}\right)\right]-\left[\frac{sin((n+0.5)\pi)-sinh((m+0.5)\pi)}{cos((n+0.5)\pi)-cosh((m+0.5)\pi)}\right]\left[cos\left(\frac{(m+0.5)\pi x}{L_x}\right)-cosh\left(\frac{(m+0.5)\pi x}{L_x}\right)\right],$$

$$Y_n(y)=\left[sin\left(\frac{(n+0.5)\pi y}{L_y}\right)-sinh\left(\frac{(n+0.5)\pi y}{L_y}\right)\right]-\left[\frac{sin((n+0.5)\pi)-sinh((n+0.5)\pi)}{cos((n+025)\pi)-cosh((n+0.5)\pi)}\right]\left[cos\left(\frac{(n+0.5)\pi y}{L_y}\right)-cosh\left(\frac{(n+0.5)\pi y}{L_y}\right)\right] \tag{25}$$

A residual algebraic statement will be produced in accordance with the Galerkin methodology by putting Equation (22) into governing Equations (A1-A7). The residual must be made to be orthogonal to the shape functions in order to guarantee the solution's accuracy. By taking the inner product of the residual with each of the form functions, the orthogonality of the residual to the shape functions can be seen. If all of the shape functions have an inner product of zero, then the residual is orthogonal to the shape functions.

$$\iint R\,(x,y)X_m(x)Y_n(y)dxdy=0,\quad m,n=1,2,3,\ldots \tag{26}$$

The nonhomogeneous algebraic equation system is represented by a (7×7) matrix via the Galerkin technique as:

$$\left(\begin{bmatrix}\alpha_{11}&\alpha_{12}&\alpha_{13}&\alpha_{14}&\alpha_{15}&\alpha_{16}&\alpha_{17}\\ \alpha_{21}&\alpha_{22}&\alpha_{23}&\alpha_{24}&\alpha_{25}&\alpha_{26}&\alpha_{27}\\ \alpha_{31}&\alpha_{32}&\alpha_{33}&\alpha_{34}&\alpha_{35}&\alpha_{36}&\alpha_{37}\\ \alpha_{41}&\alpha_{42}&\alpha_{43}&\alpha_{44}&\alpha_{45}&\alpha_{46}&\alpha_{47}\\ \alpha_{51}&\alpha_{52}&\alpha_{53}&\alpha_{54}&\alpha_{55}&\alpha_{56}&\alpha_{57}\\ \alpha_{61}&\alpha_{62}&\alpha_{63}&\alpha_{64}&\alpha_{65}&\alpha_{66}&\alpha_{67}\\ \alpha_{71}&\alpha_{72}&\alpha_{73}&\alpha_{74}&\alpha_{75}&\alpha_{76}&\alpha_{77}\end{bmatrix}+\omega^2\begin{bmatrix}\eta_{11}&0&\eta_{13}&\eta_{14}&0&0&0\\ 0&\eta_{22}&\eta_{23}&0&\eta_{24}&0&0\\ \eta_{31}&\eta_{32}&\eta_{33}&\eta_{34}&\eta_{35}&0&0\\ \eta_{41}&0&\eta_{43}&\eta_{44}&0&0&0\\ 0&\eta_{52}&\eta_{53}&0&\eta_{55}&0&0\\ 0&0&0&0&0&0&0\\ 0&0&0&0&0&0&0\end{bmatrix}\right)\begin{Bmatrix}\tilde{U}\\ \tilde{V}\\ \tilde{W}\\ \tilde{\theta}_x\\ \tilde{\theta}_y\\ \tilde{\phi}\\ \tilde{\psi}\end{Bmatrix}=\begin{Bmatrix}0\\0\\F\\0\\0\\0\\0\end{Bmatrix} \tag{27}$$

in which, $\boldsymbol{X}=\left[\bar{u}_0,\bar{v}_0,\bar{W}_0,\bar{\theta}_x,\bar{\theta}_y\right]^T$; $[\boldsymbol{a_{ij}}]$ indicates the stiffness matrix; $[\boldsymbol{\eta_{ij}}]$ expresses the mass matrix.

Furthermore, $F=\int_0^{L_x}\int_0^{L_y}Q_{mn}X_mY_nX_mY_ndxdy-\int_0^{L_x}\int_0^{L_y}Q_{mn}(e_0a)^2\left(\frac{\partial^2X_m}{\partial x^2}Y_nX_mY_n+X_m\frac{\partial^2Y_n}{\partial y^2}X_mY_n\right)dxdy,$ (28)

$$Q_{mn}=\int_{x_0-0.5a_0}^{x_0+0.5a_0}\int_{y_0-0.5b_0}^{y_0+0.5b_0}q_0X_mY_nX_mY_ndxdy\,,$$

4. Results and discussion

The numerical outcomes are displayed in this section. It is best to check the findings with the data given in certain investigations before presenting them. However, Table 1 provides a list of the many parameters used in the following (not including the verification part).

4.1 Verification study

In this case, the procedure's accuracy is tested by a series of comparisons. As a first verification study, by eliminating MEE layers, dynamic load, porosity, and strain gradient parameter, the variations of the dimensionless natural frequencies $\varpi=\omega h\sqrt{\rho/G}$ of an elastic simply supported nanoplate with uniform thickness based on the present model are determined and reported in Table 2, along with the numerical results formerly reported by Ref. [77]. The present investigation employs a FSDT to simulate the structure, whereas the cited paper utilized third-order shear deformation plate theory. Furthermore, it is worth mentioning that the minor discrepancy observed in the calculated frequencies compared to the reported results in the referenced article is due to the omission of in-plane displacements of point on the mid-plane in the equations, as mentioned in Ref. [77]. The results are fairly accurate, as can be seen from this Table.

Table 1. Material properties of the sandwich FGMP-MEE nanoplate.

Properties (MEE Layer)	$BaTiO_3-CoFe_2O_4$	
Elastic (GPa)	$c_{11}=226, c_{12}=125, c_{22}=226,$ $c_{44}=44.2, c_{55}=44.2, c_{66}=51$	
Piezoelectric (C m^{-2})	$e_{31}=-2.2, e_{32}=-2.2,$ $e_{24}=5.8, e_{15}=5.8$	
Dielectric (10^{-9}C V^{-1} m^{-1})	$k_{11}=5.64,$ $k_{22}=5.64,$ $\kappa_{33}=6.35$	
Piezomagnetic (N A^{-1} m^{-1})	$q_{31}=290.1, q_{32}=290.1,$ $q_{24}=275, q_{15}=275$	
Magnetoelectric (10^{-12}N S V^{-1} C^{-1})	$a_{11}=5.367, a_{11}=5.367,$ $a_{33}=2737.5$	
Magnetic (10^{-6}N s^2 C^{-2})	$\mu_{11}=-297,$ $\mu_{22}=-297,$ $\mu_{33}=83.5$	
Mass density (Kg m^{-3})	$\rho_m=5550$	
Properties (FGM Porous Core)	Steel (metal)	Alumina (ceramic)
Elastic (GPa)	$E=200$	$E=390$
Poisson's Ratio	$\vartheta=0.33$	$\vartheta=0.24$
Mass density (Kg m^{-3})	$\rho=7800$	$\rho=3960$

Table 2. Comparison of dimensionless natural frequency of a nanoplate.

$\frac{L_x}{h}$	e_0a	present	Ref. [77]
10	0	0.0923	0.0935
	1	0.0843	0.0854
	2	0.0782	0.0791
	3	0.0731	0.0741
	4	0.0690	0.0699
	5	0.0656	0.0666
20	0	0.0236	0.0239
	1	0.0214	0.0218
	2	0.0198	0.0202
	3	0.0185	0.0189
	4	0.0175	0.0179
	5	0.0164	0.017

Table 3. Comparison of dimensionless natural frequency of a FGM nanoplate.

B.C	p	$(e_0a)^2(nm^2)$	Study	ω_1	ω_2	ω_3
SSSS	0	0	present	0.092	0.221	0.338
			Ref. [75]	0.093	0.222	0.341
		2	present	0.078	0.157	0.210
			Ref. [75]	0.079	0.157	0.212
		4	present	0.069	0.128	0.166
			Ref. [75]	0.070	0.129	0.167
	2	0	present	0.049	0.116	0.177
			Ref. [75]	0.049	0.116	0.178
		2	present	0.041	0.082	0.110
			Ref. [75]	0.041	0.083	0.111
		4	present	0.036	0.067	0.087
			Ref. [75]	0.037	0.067	0.087
CSCS	0	0	present	0.125	0.267	0.389
			Ref. [75]	0.126	0.268	0.392
		2	present	0.104	0.184	0.235
			Ref. [75]	0.104	0.185	0.237
		4	present	0.903	0.149	0.184
			Ref. [75]	0.908	0.150	0.186
	2	0	present	0.066	0.140	0.204
			Ref. [75]	0.066	0.140	0.205
		2	present	0.054	0.097	0.123
			Ref. [75]	0.055	0.097	0.124
		4	present	0.047	0.078	0.096
			Ref. [75]	0.048	0.079	0.097
CCCC	0	0	present	0.161	0.313	0.442
			Ref. [75]	0.162	0.315	0.445
		2	present	0.132	0.212	0.261
			Ref. [75]	0.132	0.213	0.263
		4	present	0.114	0.171	0.203
			Ref. [75]	0.115	0.171	0.204
	2	0	present	0.085	0.164	0.232
			Ref. [75]	0.085	0.165	0.233
		2	present	0.069	0.111	0.137
			Ref. [75]	0.069	0.111	0.137
		4	present	0.060	0.090	0.106
			Ref. [75]	0.060	0.090	0.107

In a second comparison study, the variations of the first three dimensionless natural frequencies of the FGM nanoplate ($\frac{L_x}{L_y} = 1, L_x = 10h, l = 0$) with uniform thickness for various boundary conditions are computed using the NSGT and then compared with the findings of Ref. [75], which are shown in Table 3. The comparison in this table shows that the current results accord well with the analytical predictions in Ref. [75].

Further, by eliminating the dynamic load and FGMP core layer, the first two dimensionless natural frequencies of a simply supported MEE nanoplate $\varpi = \omega L_x\sqrt{I_0/A_{11}}$ ($\frac{L_x}{L_y} = 1, \frac{L_x}{h_m} = 15, l = 0$) versus the variations of the nonlocal parameter are obtained based on the current formulations, and the results are compared with those of Refs. [78,79] in Table 4.

Table 4. Comparison of dimensionless natural frequency of a MEE nanoplate.

Frequency	Study	$e_0a = 0$	$e_0a = 0.2$	$e_0a = 0.4$
ω_{11}	present	0.380	0.284	0.187
	Ref. [78]	0.370	0.276	0.181
	Ref. [79]	0.368	0.276	0.180
ω_{12}	present	0.928	0.538	0.311
	Ref. [78]	0.925	0.537	0.310
	Ref. [79]	0.910	0.528	0.306

Further, in Table 5, the nondimensional first natural frequency of the FGM nanoplate with uniform thickness by ignoring MEE layers, porosity, and dynamic load, is computed based on the present model and compared with those of Refs. [80,81]. An adequate degree of agreement between the outcomes has been seen.

Finally, in Table 6, based on the current model, the nondimensional first natural frequency of the isotropic plate calculated for different taper parameters and aspect ratios, and the results are contrasted with those of Ref. [82] (classical plate theory) by neglecting MEE layers, FGMP, and dynamic load. This table's comparison shows that the current findings and the analytical predictions in Ref. [82] are in good accord.

Table 5. Comparison study of dimensionless natural frequency of a FGM nanoplate.

p	l	Study	$e_0\mathrm{a}=0$	$e_0\mathrm{a}=1$	$e_0\mathrm{a}=2$	$e_0\mathrm{a}=4$
1	0	present	0.054	0.049	0.046	0.041
		Ref. [80]	0.054	0.049	0.046	0.041
		Ref. [81]	0.054	0.049	0.046	0.041
	1	present	0.059	0.054	0.050	0.044
		Ref. [80]	0.059	0.054	0.050	0.044
		Ref. [81]	0.059	0.054	0.050	0.044
	2	present	0.073	0.066	0.061	0.054
		Ref. [80]	0.072	0.066	0.061	0.054
		Ref. [81]	0.072	0.066	0.061	0.054
	4	present	0.111	0.101	0.094	0.083
		Ref. [80]	0.109	0.100	0.093	0.082
		Ref. [81]	0.111	0.101	0.094	0.083
5	0	present	0.044	0.040	0.037	0.033
		Ref. [80]	0.044	0.040	0.037	0.033
		Ref. [81]	0.044	0.040	0.037	0.033
	1	present	0.048	0.044	0.040	0.036
		Ref. [80]	0.048	0.044	0.040	0.036
		Ref. [81]	0.048	0.044	0.040	0.036
	2	present	0.058	0.053	0.049	0.044
		Ref. [80]	0.058	0.053	0.049	0.044
		Ref. [81]	0.058	0.053	0.049	0.044
	4	present	0.090	0.082	0.075	0.067
		Ref. [80]	0.088	0.081	0.074	0.066
		Ref. [81]	0.089	0.082	0.075	0.067
10	0	present	0.041	0.038	0.035	0.031
		Ref. [80]	0.042	0.038	0.035	0.031
		Ref. [81]	0.041	0.038	0.035	0.031
	1	present	0.045	0.041	0.038	0.034
		Ref. [80]	0.045	0.041	0.038	0.034
		Ref. [81]	0.045	0.041	0.038	0.034
	2	present	0.055	0.051	0.047	0.041
		Ref. [80]	0.055	0.051	0.047	0.041
		Ref. [81]	0.055	0.051	0.047	0.041
	4	present	0.084	0.078	0.072	0.063
		Ref. [80]	0.084	0.077	0.071	0.062
		Ref. [81]	0.085	0.078	0.072	0.063

4.2 Main results

Here, a series of numerical simulations are used to figure out how effective factors affect the free and forced vibration of the FGMP-MEE nanoplate. The considered quantities include material gradient index, nonlocal and strain gradient parameters, initial magnetic and electric potentials, and porosity coefficients. It is assumed that $h_0 = 0.4\mathrm{nm}, h_m = 0.2\mathrm{nm}, L_x = L_y = 10\mathrm{nm}, x_0 = \frac{L_x}{5}, y_0 = \frac{L_y}{5}, a_0 = \frac{L_x}{5}, b_0 = \frac{L_y}{5}$.

In addition, the nonlocal and strain gradient parameters that were used in this analysis were chosen based on a certain range that was published in the research that was done on nonlocal elasticity and strain gradient theories. Typically, calibration processes using either molecular dynamics simulations or empirical approaches were used to get the aforementioned values.

Table 6. Nondimensional first natural frequency of the isotropic plate with a thickness that changes linearly in one direction.

B.C	Taper Parameter α	Aspect Ratio	Ref. [82]	Present
SSSS	0.25	0.5	13.9359	13.9359
		1	22.3184	22.3184
		2	55.7438	55.7438
	0.5	0.5	15.6248	15.6248
		1	25.0742	25.0742
		2	62.4994	62.4993
	1	0.5	19.1764	19.1764
		1	30.9245	30.9245
		2	76.7057	76.7057
CCSS	0.25	0.5	21.3439	21.3436
		1	32.7193	32.7190
		2	84.2476	84.2475
	0.5	0.5	24.2965	24.2964
		1	37.2871	37.2870
		2	95.2379	95.2377
	1	0.5	30.3541	30.3538
		1	46.7716	46.7715
		2	118.3476	118.3475

4.2.1 Free vibration

Depicted in Fig. 2 is the influence of the material gradient index on the variations of the first natural frequency (GHz) of the sandwich FGMP-MEE nanoplate for linearly and parabolically varying thickness under different boundary conditions (SSSS, CSCS, CCCC) when $p = 1$, $\zeta = 0, \phi_0 = 0, \psi_0 = 0$. It should be noted that in this figure, various classical and non-classical theories, *i.e.*, NSGT ($l \neq 0$, $(e_0 a) \neq 0$), SGT ($l \neq 0$, $(e_0 a) = 0$), NT ($l = 0$, $(e_0 a) \neq 0$) called NT, and CT ($l = 0$, $(e_0 a) = 0$) are considered. However, it can be observed that the boundary conditions have important effects on the variations of the natural frequencies. It may be deduced that for a given volume of sandwich

nanoplate application, a sandwich nanoplate with bi-directional thickness variation is preferable to a sandwich plate of even thickness in order to achieve the maximal frequency. Due to the increased rigidity and decreased deformation of bidirectional nanoplates compared to unidirectional nanoplates, the natural frequency of a sandwich FGMP-MEE nanoplate with variable thickness in two directions is higher than that of a nanoplate with variable thickness in one direction. In contrast to a nanoplate with a parabolically varying thickness, which has a mass distribution that is more uniformly distributed throughout the plate, a nanoplate with a linearly varying thickness has a mass distribution that is concentrated towards the plate's edges. Moreover, a nanoplate's stiffness is less uniformly distributed when its thickness varies linearly as opposed to parabolically. This is because the linear variation in thickness results in non-uniform bending stiffness across the plate. In contrast, a plate with a parabolically varying thickness has a more uniform bending stiffness. The non-uniform stiffness and mass distribution of a sandwich nanoplate with a linearly varying thickness can lead to a higher natural frequency compared to a sandwich nanoplate with a parabolically varying thickness. Furthermore, the natural frequency is decreased as a result of the transition from a ceramic to a metallic state, which exhibits an increase in the FG index and a decrease in stiffness. Furthermore, according to the effects of nonlocal and strain gradient parameters and how to use these parameters in nonclassical theories, the natural frequency according to these theories are as NT <CT <NSGT <SGT.

Table 7 depicts the effects of the electric voltage, magnetic potential, and porosity coefficient on the fundamental frequency (GHz) of simply supported sandwich FGMP-MEE nanoplate for linearly varying thickness under different porosity distributions when $p = 1, l = 0, (e_0a) = 0, \alpha = 0.5, \beta = 0$. In terms of the porosity coefficient, regardless of the porosity pattern, one notices a declining frequency with an increasing porosity coefficient. As the porosity coefficient goes up, the nanoplate's effective density goes down, which makes it less stiff. This is because the pores or voids in the plate reduce the amount of solid material present, which in turn decreases the plate's resistance to deformation. Therefore, the sandwich FGM-MEE nanoplate's natural frequency drops. In summary, the porosity dispersion of a sandwich porous nanoplate can significantly affect its natural frequencies. Even porosity dispersion leads to evenly spaced natural frequencies, while uneven and logarithmic uneven porosity dispersion result in irregular and complex frequency patterns. On the other hand, a sandwich nanoplate with even porosity distribution has a more consistent distribution of pores, which leads to a more uniform response to external vibrations and a higher natural frequency overall. In a variety of applications, including acoustic filters, heat exchangers, and fluid flow control systems, this can increase the sandwich smart nanoplate's reliability and efficiency. Furthermore, as noted in Table 7, the natural frequency decreases when the electric voltage rises due to an increase in the system's deformation. This is because the increased deformation of the sandwich nanoplate results in a decrease in the stiffness of the sandwich nanoplate, which in turn reduces the natural frequency. This phenomenon is important in the design and operation of piezoelectric devices, where the natural frequency of the device is an important parameter that needs to be controlled and optimized. As is evident, raising the external magnetic potential increases the frequency values. The magnetic field in the MEE nanoplate gets stronger as the magnetic potential rises, which in turn leads the material's magnetic dipoles to line up with the field direction. Because the magnetic forces between the dipoles balance out the material's deformation, this alignment of the magnetic dipoles increases the plate's stiffness.

4.2.2 Forced vibration

Figure 3 demonstrates the variations of the dynamic deflection response of the sandwich FGMP-MEE nanoplate for linearly and parabolically varying thickness under different boundary conditions (SSSS, CSCS, CCCC) when $p = 1,\ \zeta = 0, \phi_0 = 0, \psi_0 = 0, l = 0, (e_0a) = 0$. In general, a nanoplate that varies in thickness in only one direction would have a lower natural frequency and would resonate at a lower frequency when compared to a nanoplate that varies in thickness in two directions. Due to the distribution of the sandwich nanoplate's mass and stiffness, a nanoplate with a parabolically varying

Table 7. Effects of the electric voltage, magnetic potential, and porosity coefficient on the fundamental frequency (GHz) of simply supported sandwich FGMP-MEE nanoplate for different porosity distributions.

Porosity distribution	ζ	ϕ_0(V)			ψ_0(A)		
		0	0.1	0.2	0	0.01	0.02
Even porosity	0	0.2864	0.1934	0.0877	0.2864	0.4657	0.5931
	0.2	0.2811	0.1875	0.0789	0.2811	0.4546	0.5782
	0.4	0.2766	0.1769	0.0705	0.2766	0.4444	0.5645
Uneven porosity	0	0.2864	0.1934	0.0877	0.2864	0.4657	0.5931
	0.2	0.2802	0.1715	0.0683	0.2864	0.4468	0.5664
	0.4	0.2750	0.1626	0.0614	0.2750	0.4308	0.5437
Logarithmic uneven porosity	0	0.2864	0.1934	0.0877	0.2864	0.4657	0.5931
	0.2	0.2807	0.1834	0.0755	0.2807	0.4517	0.5767
	0.4	0.2757	0.1726	0.0681	0.2757	0.4403	56.051

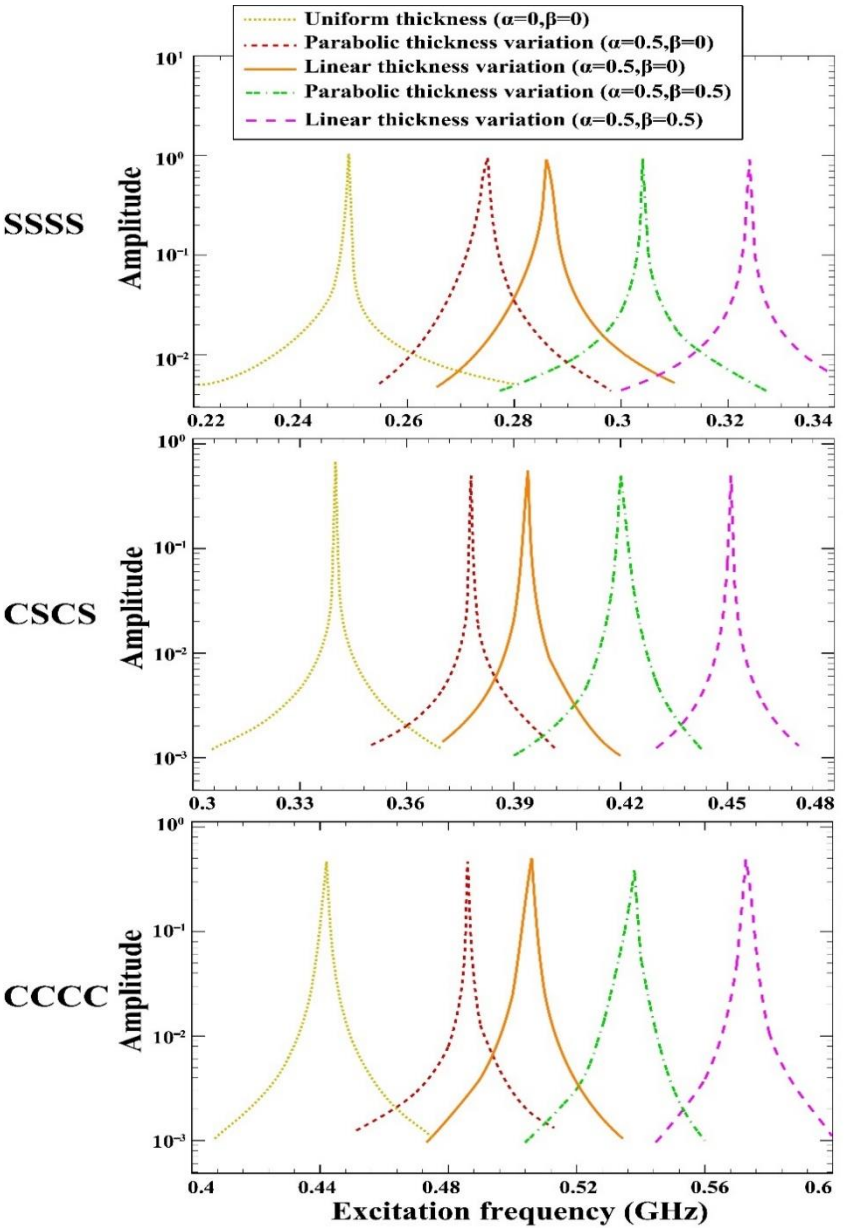

Fig. 3 Dynamic deflection response of the sandwich FGMP-MEE nanoplate for linearly and parabolically varying thickness.

thickness has a lower resonance frequency than a nanoplate with a linearly varying thickness. As a result of the mass and stiffness being concentrated in the plate's center, which has a parabolically changing thickness, the resonance frequency is reduced. In contrast, a nanoplate with a linearly varying thickness has a more uniform distribution of mass and stiffness, which results in a higher resonance frequency.

Figure 4 exhibits the effect of the nonlocal parameter on the dynamic behavior of the sandwich FGMP-MEE nanoplate with linearly and parabolically varying thickness versus the resonance frequency when $p = 1,\ \zeta = 0, \phi_0 = 0, \psi_0 = 0, l = 0, \alpha = 0.5, \beta = 0$. The resonance frequency of the nanoplate decreases with increasing nonlocal term. This is because the stiffness of the nanoplate decreases when its effective mass grows due to a rise in the nonlocal parameter. It should be noted that the clamped boundary condition imposes a stronger constraint on the deformation of the sandwich nanoplate. Because of this, the nonlocal effects, which are caused by the nonlocal interactions that occur between adjacent atoms or molecules, have a stronger impact on the frequency response of the sandwich nanoplate when it is subjected to a clamped boundary condition.

Figure 5 exhibits the effect of the strain gradient parameter on the dynamic behavior of the sandwich FGMP-MEE nanoplate with linearly and parabolically varying thickness versus the resonance frequency when $p = 1,\ \zeta = 0, \phi_0 = 0, \psi_0 = 0, (e_0 a) = 0, \alpha = 0.5, \beta = 0$. From this figure, it is obvious that the resonance frequency of the sandwich nanoplate increases with increasing strain gradient parameter. With a rise in the strain gradient parameter, a nanoplate becomes stiffer. The resonance frequency of the nanoplate rises as a result of this increase in stiffness.

Figure 6 exhibits the effects of the power law index on the dynamic behavior of a simply supported sandwich FGMP-

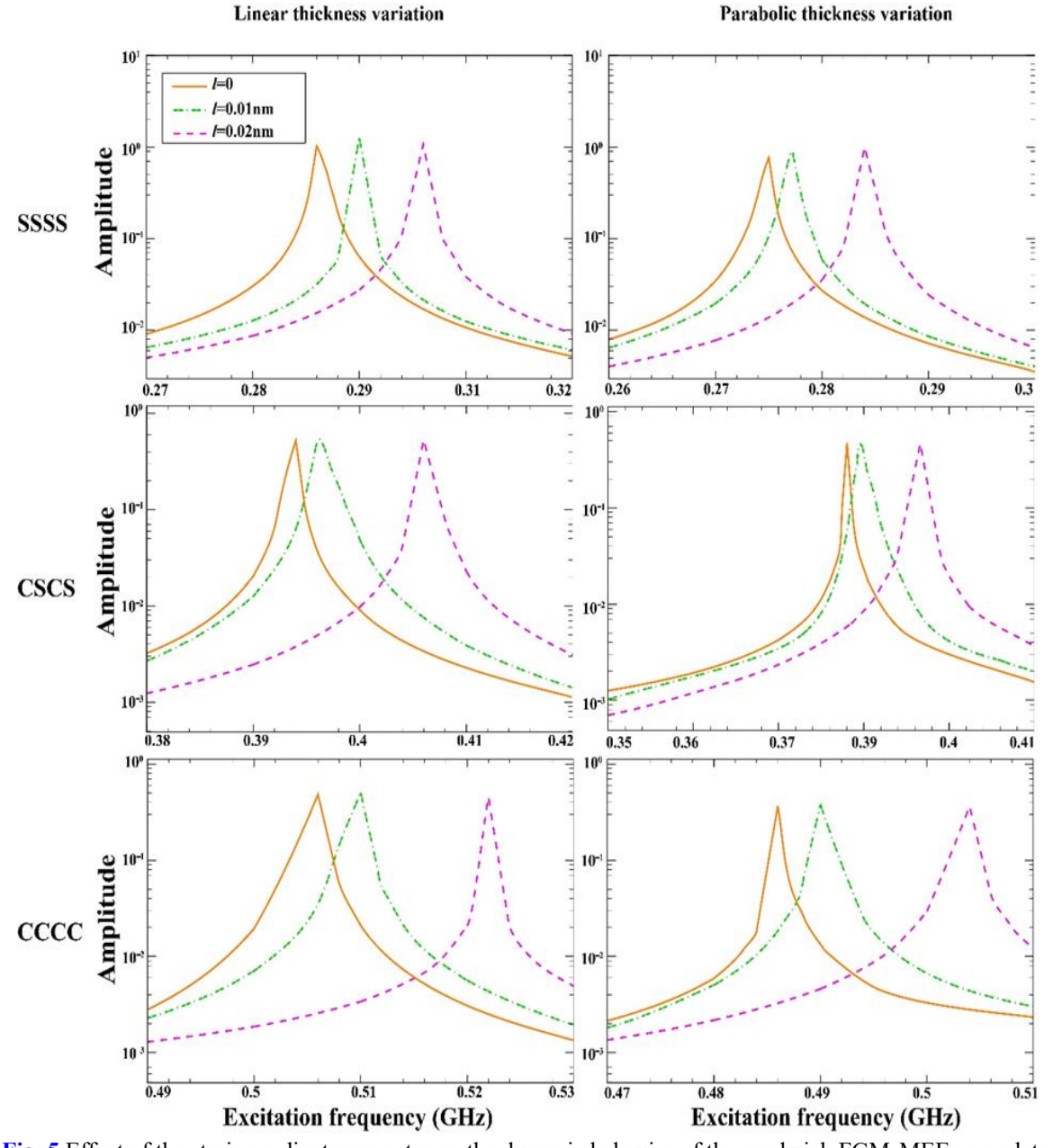

Fig. 5 Effect of the strain gradient parameter on the dynamic behavior of the sandwich FGM-MEE nanoplate.

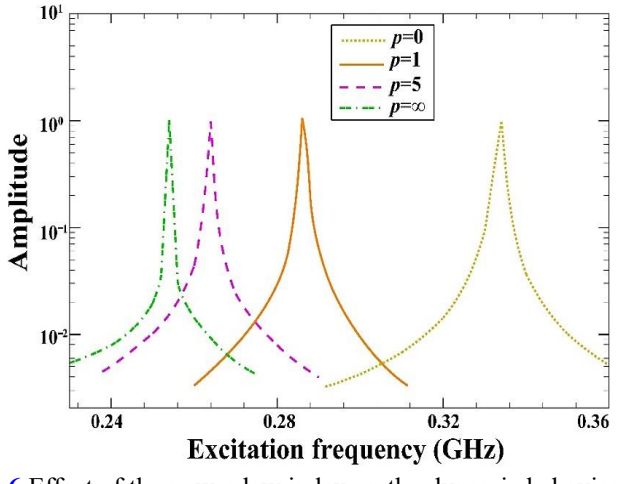

Fig. 6 Effect of the power law index on the dynamic behavior of the sandwich PFGM-MEE nanoplate.

MEE nanoplate with linearly varying thickness versus the resonance frequency when $\zeta = 0, \phi_0 = 0, \psi_0 = 0, (e_0 a) = 0, l = 0, \alpha = 0.5, \beta = 0$. The relationship between the material gradient index and the mechanical properties of the core layer is of crucial importance. It is inferred that the mechanical properties of the core layer trend towards metal characteristics as the material gradient index rises; as a result, the stiffness of the structure lowers, the resonance phenomena occur at a lower frequency, and the amplitude of the dynamic response rises.

Figure 7 describes the variations of the dynamic deflection versus different porosity distributions for the case of a simply supported sandwich FGMP-MEE nanoplate with linearly varying thickness versus the resonance frequency when $p = 1, \phi_0 = 0, \psi_0 = 0, (e_0 a) = 0, l = 0, \alpha = 0.5, \beta = 0$. As is obvious, with increasing porosity, the dynamic

response of the system rises. This behavior is attributable to the decrease in structural stiffness as porosity increases, which causes the system's dynamic response to increase. The volume of the voids in a porous nanoplate increases and the volume of the solid material decreases as the porosity coefficient of the plate rises. The sandwich FGMP-MEE nanoplate's effective stiffness consequently decreases, which decreases the resonance frequency of the plate.

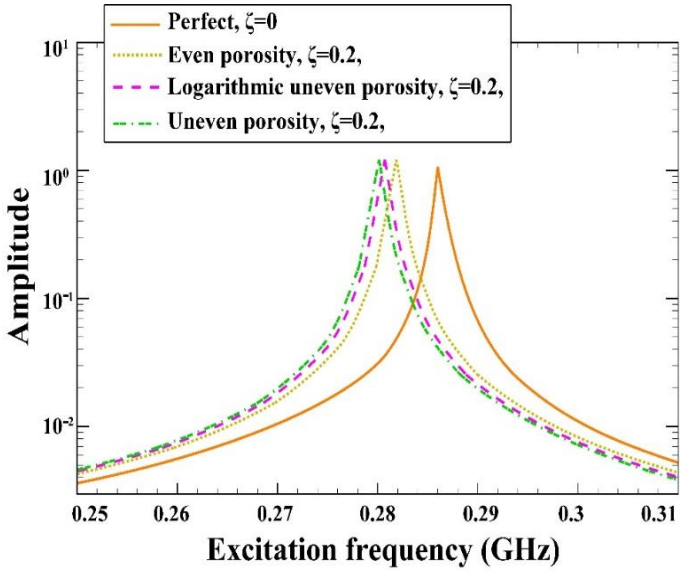

Fig. 7 Effect of the different porosity distributions on the dynamic behavior of the sandwich FGMP-MEE nanoplate.

The effects of the initial electric and magnetic potentials on the forced vibration behavior of a simply supported sandwich FGMP-MEE nanoplate with linearly varying thickness versus the resonance frequency are respectively shown in Figs. 8 and 9 when $p = 1, \zeta = 0, (e_0 a) = 0, l = 0, \alpha = 0.5, \beta = 0$. One can see that the electric and magnetic potentials can significantly affect the resonance frequencies and the dynamic deflections. Actually, electric and magnetic potentials are appropriate tools to enhance and improve the resonance area of the nanostructures. This control over resonance frequencies opens up opportunities for tuning the behavior of nanostructures to meet specific requirements in various applications. For example, by adjusting the electric potential, one can shift the resonance frequencies to desired ranges, enabling enhanced performance in sensors, actuators, and energy harvesting devices.

Figure 10 illustrates the variations in dynamic deflection of a simply supported sandwich FGMP-MEE nanoplate with linearly varying thickness for different areas of uniform dynamic load when $p = 1, \zeta = 0, (e_0 a) = 0, l = 0, \phi_0 = 0, \psi_0 = 0, \alpha = 0.5, \beta = 0$. It can be inferred that an increase in the region of the applied transverse load causes an increase in the dynamic deflection. In fact, the area of frequency-response plots becomes wider. It should be noted that the resonance frequency is not affected by the geometrical parameters of the uniform dynamic load.

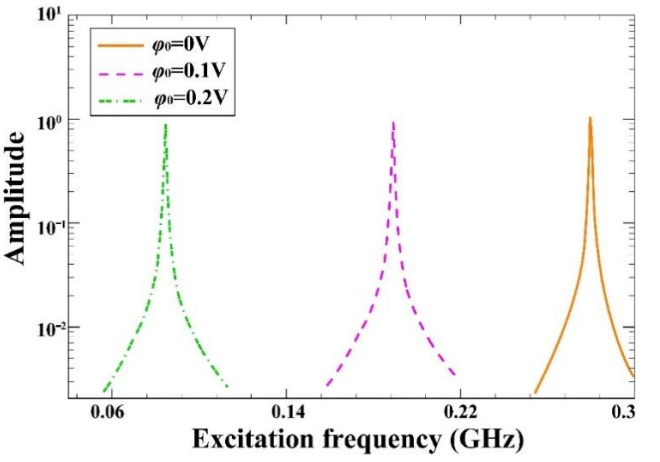

Fig. 8 Effect of the electric voltage on the dynamic behavior of the sandwich FGMP-MEE nanoplate.

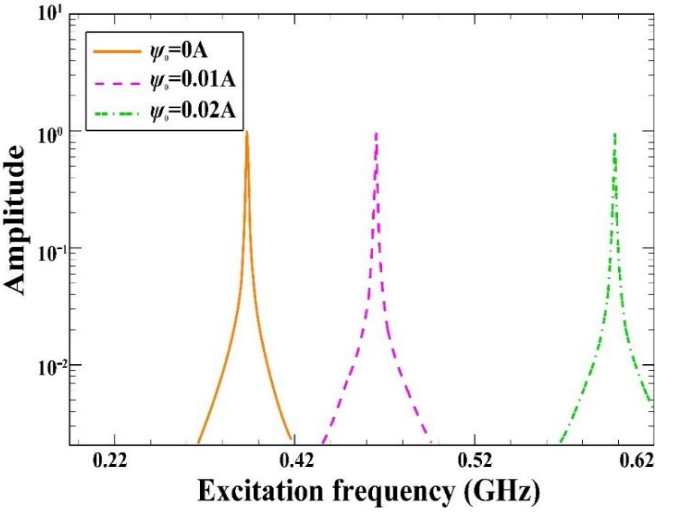

Fig. 9 Effect of the magnetic potential on the dynamic behavior of the sandwich FGMP-MEE nanoplate.

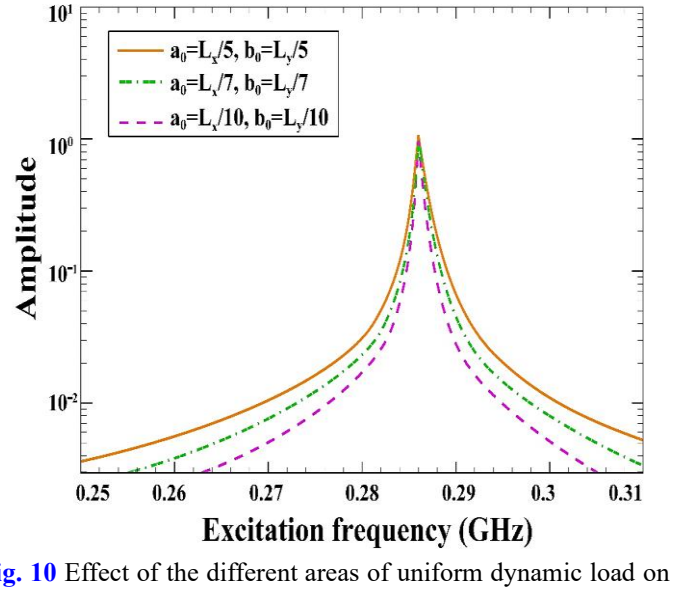

Fig. 10 Effect of the different areas of uniform dynamic load on the dynamic behavior of the sandwich FGMP-MEE nanoplate.

5. Conclusions

For the purpose of studying the free and forced vibration analysis of the sandwich MEE nanoplates with FGMP of linearly or parabolically varying thickness core layer under initial external electric and magnetic potentials for various boundary conditions, an analytical strategy based on the nonlocal strain gradient in conjunction with the FSDT has been established. The FGMP layer's attributes are spread out in an even, an uneven, and a logarithmically uneven way based on a specific rule-of-mixture relation. Hamilton's principle was used to construct the dynamic structural equations, which were then analytically solved using the Galerkin technique. Through a comparison with other accessible data from previous studies, the generated solution is examined in terms of its correctness and precision. The effects of the bidirectional taper constants, initial electric and magnetic potentials, porosity distributions, FG index, and nonlocal and strain gradient factors on free and forced vibration are shown by parameter analyses. The following are some of the most notable findings from this study:

- The non-uniform stiffness and mass distribution of a sandwich nanoplate with a linearly varying thickness can lead to a higher natural frequency compared to a sandwich nanoplate with a parabolically varying thickness.
- Even porosity dispersion leads to evenly spaced natural frequencies, while uneven and logarithmic uneven porosity dispersion result in irregular and complex frequency patterns.
- The resonance frequency decreases when the electric voltage rises due to an increase in the system's deformation. This is because the increased deformation of the sandwich nanoplate results in a decrease in the stiffness of the sandwich nanoplate, which in turn reduces the resonance frequency.
- The effects of the nonlocal and strain gradient parameters in the CCCC boundary condition on the resonance frequency changes are greater than in the SSSS boundary condition.
- The mechanical properties of the core layer trend towards metal characteristics as the material gradient index rises; as a result, the stiffness of the structure lowers, and the resonance phenomena occur at a lower frequency.

Finally, here, we will include a discussion on the future directions of our work. We will explore the potential of incorporating active control techniques, machine learning algorithms, and optimization algorithms to further enhance the performance of the sandwich smart MEE nanoplates with FGMP core layers. By leveraging active control strategies along with machine learning and optimization algorithms, we aim to develop advanced control methodologies that can optimize the vibration characteristics, energy efficiency, and overall performance of the nanoplates. This direction of research has the potential to significantly contribute to the field of active control of smart materials and structures.

Acknowledgments

This study was supported by Thammasat Postdoctoral Fellowship, Thammasat University research Division, Thammasat University. Also, This research is supported by the Thammasat University Research Unit in Structural and Foundation Engineering, Thammasat University. In addition, the financial support from Thailand Science Research and Innovation (TSRI) Basic Research Fund: Fiscal year 2023 and King Mongkut's University of Technology Thonburi (KMUTT) Research Fund are gratefully acknowledged.

Conflict of Interest

There is no conflict of interest.

Supporting Information

Not applicable.

APPENDIX A

The size-dependent equilibrium equations governing a sandwich FGMP-MEE nanoplate can be derived as follows:

$$\delta u_0 \to \left[1 - l^2\left(\frac{\partial^2}{\partial x^2} + \frac{\partial^2}{\partial y^2}\right)\right]\left\{A_{11}\frac{\partial^2 u_0}{\partial x^2} + \frac{\partial A_{11}}{\partial x}\frac{\partial u_0}{\partial x} + B_{11}\frac{\partial^2 \theta_x}{\partial x^2} + \frac{\partial B_{11}}{\partial x}\frac{\partial \theta_x}{\partial x} + A_{12}\frac{\partial^2 v_0}{\partial x \partial y} + \frac{\partial A_{12}}{\partial x}\frac{\partial v_0}{\partial y} + B_{12}\frac{\partial^2 \theta_y}{\partial x \partial y} + \frac{\partial B_{12}}{\partial x}\frac{\partial \theta_y}{\partial y} + A_{66}\left(\frac{\partial^2 u_0}{\partial y^2} + \frac{\partial^2 v_0}{\partial x \partial y}\right) + \frac{\partial A_{66}}{\partial y}\left(\frac{\partial u_0}{\partial y} + \frac{\partial v_0}{\partial x}\right) + B_{66}\left(\frac{\partial^2 \theta_x}{\partial y^2} + \frac{\partial^2 \theta_y}{\partial x \partial y}\right) + \frac{\partial B_{66}}{\partial y}\left(\frac{\partial \theta_x}{\partial y} + \frac{\partial \theta_y}{\partial x}\right) + F_{31}\frac{\partial \Phi}{\partial x} + \frac{\partial F_{31}}{\partial x}\Phi + G_{31}\frac{\partial \Psi}{\partial x} + \frac{\partial G_{31}}{\partial x}\Psi\right\} = \left[1 - (e_0 a)^2\left(\frac{\partial^2}{\partial x^2} + \frac{\partial^2}{\partial y^2}\right)\right](I_0 \ddot{u_0} + I_1 \ddot{\theta_x}), \tag{A1}$$

$$\delta v_0 \to \left[1 - l^2\left(\frac{\partial^2}{\partial x^2} + \frac{\partial^2}{\partial y^2}\right)\right]\left\{A_{12}\frac{\partial^2 u_0}{\partial x \partial y} + \frac{\partial A_{12}}{\partial y}\frac{\partial u_0}{\partial x} + B_{12}\frac{\partial^2 \theta_x}{\partial x \partial y} + \frac{\partial B_{12}}{\partial y}\frac{\partial \theta_x}{\partial x} + A_{11}\frac{\partial^2 v_0}{\partial y^2} + \frac{\partial A_{11}}{\partial y}\frac{\partial v_0}{\partial y} + B_{11}\frac{\partial^2 \theta_y}{\partial y^2} + \frac{\partial B_{11}}{\partial y}\frac{\partial \theta_y}{\partial y} + A_{66}\left(\frac{\partial^2 u_0}{\partial x \partial y} + \frac{\partial^2 v_0}{\partial x^2}\right) + \frac{\partial A_{66}}{\partial x}\left(\frac{\partial u_0}{\partial y} + \frac{\partial v_0}{\partial x}\right) + B_{66}\left(\frac{\partial^2 \theta_x}{\partial x \partial y} + \frac{\partial^2 \theta_y}{\partial y^2}\right) + \frac{\partial B_{66}}{\partial x}\left(\frac{\partial \theta_x}{\partial y} + \frac{\partial \theta_y}{\partial x}\right) + F_{31}\frac{\partial \Phi}{\partial y} + \frac{\partial F_{31}}{\partial y}\Phi + G_{31}\frac{\partial \Psi}{\partial y} + \frac{\partial G_{31}}{\partial y}\Psi\right\} = \left[1 - (e_0 a)^2\left(\frac{\partial^2}{\partial x^2} + \frac{\partial^2}{\partial y^2}\right)\right](I_0 \ddot{v_0} + I_1 \ddot{\theta_y}), \tag{A2}$$

$$\delta W_0 \to \left[1 - l^2\left(\frac{\partial^2}{\partial x^2} + \frac{\partial^2}{\partial y^2}\right)\right]\left\{k_s A_{44}\left(\frac{\partial \theta_x}{\partial x} + \frac{\partial^2 W_0}{\partial x^2}\right) + k_s\frac{\partial A_{44}}{\partial x}\left(\theta_x + \frac{\partial W_0}{\partial x}\right) + k_s A_{44}\left(\frac{\partial \theta_y}{\partial y} + \frac{\partial^2 W_0}{\partial y^2}\right) + k_s\frac{\partial A_{44}}{\partial y}\left(\theta_y + \frac{\partial W_0}{\partial y}\right) + k_s\bar{F}_{15}\frac{\partial \Phi}{\partial x} + k_s\frac{\partial \bar{F}_{15}}{\partial x}\Phi - k_s F_{15}\frac{\partial^2 \Phi}{\partial x^2} - k_s\frac{\partial F_{15}}{\partial x}\frac{\partial \Phi}{\partial x} + k_s\bar{G}_{15}\frac{\partial \Psi}{\partial x} + k_s\frac{\partial \bar{G}_{15}}{\partial x}\Psi - k_s G_{15}\frac{\partial^2 \Psi}{\partial x^2} - k_s\frac{\partial G_{15}}{\partial x}\frac{\partial \Psi}{\partial x} + k_s\bar{F}_{24}\frac{\partial \Phi}{\partial y} + k_s\frac{\partial \bar{F}_{24}}{\partial y}\Phi - k_s F_{24}\frac{\partial^2 \Phi}{\partial y^2} - k_s\frac{\partial F_{24}}{\partial y}\frac{\partial \Phi}{\partial y} + k_s\bar{G}_{24}\frac{\partial \Psi}{\partial y} + k_s\frac{\partial \bar{G}_{24}}{\partial y}\Psi - k_s G_{24}\frac{\partial^2 \Psi}{\partial y^2} - k_s\frac{\partial G_{24}}{\partial y}\frac{\partial \Psi}{\partial y}\right\} = \left[1 - (e_0 a)^2\left(\frac{\partial^2}{\partial x^2} + \right.\right. \tag{A3}$$

$$\tag{A4}$$

$$\tag{A5}$$

$$\tag{A6}$$

$$\tag{A7}$$

$$\frac{\partial^2}{\partial y^2}\Big)\Big]\Big\{q_{DYN}+I_0\ddot{W}_0-N_E\Big(\frac{\partial^2 W_0}{\partial x^2}+\frac{\partial^2 W_0}{\partial y^2}\Big)-N_M\Big(\frac{\partial^2 W_0}{\partial x^2}+\frac{\partial^2 W_0}{\partial y^2}\Big)\Big\},$$

$$\delta\theta_x \to \Big[1-l^2\Big(\frac{\partial^2}{\partial x^2}+\frac{\partial^2}{\partial y^2}\Big)\Big]\Big\{B_{11}\frac{\partial^2 u_0}{\partial x^2}+\frac{\partial B_{11}}{\partial x}\frac{\partial u_0}{\partial x}+H_{11}\frac{\partial^2\theta_x}{\partial x^2}+\frac{\partial H_{11}}{\partial x}\frac{\partial\theta_x}{\partial x}+B_{12}\frac{\partial^2 v_0}{\partial x\partial y}+\frac{\partial B_{12}}{\partial x}\frac{\partial v_0}{\partial y}+H_{12}\frac{\partial^2\theta_y}{\partial x\partial y}+\frac{\partial H_{12}}{\partial x}\frac{\partial\theta_y}{\partial y}+B_{66}\Big(\frac{\partial^2 u_0}{\partial y^2}+\frac{\partial^2 v_0}{\partial x\partial y}\Big)+\frac{\partial B_{66}}{\partial y}\Big(\frac{\partial u_0}{\partial y}+\frac{\partial v_0}{\partial x}\Big)+H_{66}\Big(\frac{\partial^2\theta_x}{\partial y^2}+\frac{\partial^2\theta_y}{\partial x\partial y}\Big)+\frac{\partial H_{66}}{\partial y}\Big(\frac{\partial\theta_x}{\partial y}+\frac{\partial\theta_y}{\partial x}\Big)-k_sA_{44}\Big(\theta_x+\frac{\partial W_0}{\partial x}\Big)+\bar{F}_{31}\frac{\partial\Phi}{\partial x}+\frac{\partial\bar{F}_{31}}{\partial x}\Phi+\bar{G}_{31}\frac{\partial\Psi}{\partial x}+\frac{\partial\bar{G}_{31}}{\partial x}\Psi-k_s\bar{F}_{15}\Phi+k_sF_{15}\frac{\partial\Phi}{\partial x}-k_s\bar{G}_{15}\Psi+k_sG_{15}\frac{\partial\Psi}{\partial x}\Big\}=\Big[1-(e_0a)^2\Big(\frac{\partial^2}{\partial x^2}+\frac{\partial^2}{\partial y^2}\Big)\Big](I_1\ddot{u}_0+I_2\ddot{\theta}_x),$$

$$\delta\theta_y \to \Big[1-l^2\Big(\frac{\partial^2}{\partial x^2}+\frac{\partial^2}{\partial y^2}\Big)\Big]\Big\{B_{12}\frac{\partial^2 u_0}{\partial x\partial y}+\frac{\partial B_{12}}{\partial y}\frac{\partial u_0}{\partial x}+H_{12}\frac{\partial^2\theta_x}{\partial x\partial y}+\frac{\partial H_{12}}{\partial y}\frac{\partial\theta_x}{\partial x}+B_{22}\frac{\partial^2 v_0}{\partial y^2}+\frac{\partial B_{22}}{\partial y}\frac{\partial v_0}{\partial y}+H_{22}\frac{\partial^2\theta_y}{\partial y^2}+\frac{\partial H_{22}}{\partial y}\frac{\partial\theta_y}{\partial y}+B_{66}\Big(\frac{\partial^2 u_0}{\partial x\partial y}+\frac{\partial^2 v_0}{\partial x^2}\Big)+\frac{\partial B_{66}}{\partial x}\Big(\frac{\partial u_0}{\partial y}+\frac{\partial v_0}{\partial x}\Big)+H_{66}\Big(\frac{\partial^2\theta_x}{\partial x\partial y}+\frac{\partial^2\theta_y}{\partial y^2}\Big)+\frac{\partial H_{66}}{\partial x}\Big(\frac{\partial\theta_x}{\partial y}+\frac{\partial\theta_y}{\partial x}\Big)-k_sA_{66}\Big(\theta_y+\frac{\partial W_0}{\partial y}\Big)+\bar{F}_{31}\frac{\partial\Phi}{\partial y}+\frac{\partial\bar{F}_{31}}{\partial y}\Phi+\bar{G}_{31}\frac{\partial\Psi}{\partial y}+\frac{\partial\bar{G}_{31}}{\partial y}\Psi-k_s\bar{F}_{24}\Phi+k_sF_{24}\frac{\partial\Phi}{\partial y}-k_s\bar{G}_{24}\Psi+k_sG_{24}\frac{\partial\Psi}{\partial y}\Big\}=\Big[1-(e_0a)^2\Big(\frac{\partial^2}{\partial x^2}+\frac{\partial^2}{\partial y^2}\Big)\Big]\Big(\bar{I}_1\ddot{v}_0+\bar{I}_2\ddot{\theta}_y-C_1\bar{I}_4\frac{\partial\ddot{W}_0}{\partial y}\Big),$$

$$\delta\Phi \to \Big[1-l^2\Big(\frac{\partial^2}{\partial x^2}+\frac{\partial^2}{\partial y^2}\Big)\Big]\Big\{F_{31}\Big(\frac{\partial u_0}{\partial x}+\frac{\partial v_0}{\partial y}\Big)+\bar{F}_{31}\Big(\frac{\partial\theta_x}{\partial x}+\frac{\partial\theta_y}{\partial y}\Big)+F_{15}\Big(\frac{\partial\theta_x}{\partial x}+\frac{\partial^2 W_0}{\partial x^2}\Big)+F_{24}\Big(\frac{\partial\theta_y}{\partial y}+\frac{\partial^2 W_0}{\partial y^2}\Big)-F_{16}\Big(\theta_x+\frac{\partial W_0}{\partial x}\Big)-F_{26}\Big(\theta_y+\frac{\partial W_0}{\partial y}\Big)+(F_1-F_2-F_3+\bar{F}_1-\bar{F}_2-\bar{F}_3-F_{33})\Phi-F_4\frac{\partial\Phi}{\partial x}+F_5\frac{\partial^2\Phi}{\partial x^2}-\bar{F}_4\frac{\partial\Phi}{\partial y}+\bar{F}_5\frac{\partial^2\Phi}{\partial y^2}+(F_6-F_7-F_8+\bar{F}_6-\bar{F}_7-\bar{F}_8-G_{33})\Psi-F_9\frac{\partial\Psi}{\partial x}+F_{10}\frac{\partial^2\Psi}{\partial x^2}-\bar{F}_9\frac{\partial\Psi}{\partial y}+\bar{F}_{10}\frac{\partial^2\Psi}{\partial y^2}\Big\}=0,$$

$$\delta\Psi \to \Big[1-l^2\Big(\frac{\partial^2}{\partial x^2}+\frac{\partial^2}{\partial y^2}\Big)\Big]\Big\{G_{31}\Big(\frac{\partial u_0}{\partial x}+\frac{\partial v_0}{\partial y}\Big)+\bar{G}_{31}\Big(\frac{\partial\theta_x}{\partial x}+\frac{\partial\theta_y}{\partial y}\Big)+G_{15}\Big(\frac{\partial\theta_x}{\partial x}+\frac{\partial^2 W_0}{\partial x^2}\Big)+G_{24}\Big(\frac{\partial\theta_y}{\partial y}+\frac{\partial^2 W_0}{\partial y^2}\Big)-G_{16}\Big(\theta_x+\frac{\partial W_0}{\partial x}\Big)-G_{26}\Big(\theta_y+\frac{\partial W_0}{\partial y}\Big)+(F_6-F_7-F_8+\bar{F}_6-\bar{F}_7-\bar{F}_8-G_{33})\Phi-F_9\frac{\partial\Phi}{\partial x}+F_{10}\frac{\partial^2\Phi}{\partial x^2}-\bar{F}_9\frac{\partial\Phi}{\partial y}+\bar{F}_{10}\frac{\partial^2\Phi}{\partial y^2}+(F_{11}-F_{12}-F_{13}+\bar{F}_{11}-\bar{F}_{12}-\bar{F}_{13}-P_{33})\Psi-F_{14}\frac{\partial\Psi}{\partial x}+F_{15}\frac{\partial^2\Psi}{\partial x^2}-\bar{F}_{14}\frac{\partial\Psi}{\partial y}+\bar{F}_{15}\frac{\partial^2\Psi}{\partial y^2}\Big\}=0,$$

where each of the coefficients in equations (A1-A7) can be presented as:

$$(A_{11},B_{11},H_{11})=\int_{-h_m-h(x,y)/2}^{-h(x,y)/2}\underline{C}_{11}(1,z,z^2)dz+\int_{-h(x,y)/2}^{h(x,y)/2}Q_{11}(z)(1,z,z^2)dz+\int_{h/2}^{h/2+h_m}\underline{C}_{11}(1,z,z^2)dz,$$

$$(A_{12},B_{12},H_{12})=\int_{-h_m-h(x,y)/2}^{-h(x,y)/2}\underline{C}_{12}(1,z,z^2)dz+\int_{-h(x,y)/2}^{h(x,y)/2}Q_{12}(z)(1,z,z^2)dz+\int_{h/2}^{h/2+h_m}\underline{C}_{12}(1,z,z^2)dz,$$

$$(A_{22},B_{22},H_{22})=\int_{-h_m-h(x,y)/2}^{-h(x,y)/2}\underline{C}_{22}(1,z,z^2)dz+\int_{-h(x,y)/2}^{h(x,y)/2}Q_{22}(z)(1,z,z^2)dz+\int_{h(x,y)/2}^{h(x,y)/2+h_m}\underline{C}_{22}(1,z,z^2)dz,$$

$$(A_{44},B_{44},H_{44})=\int_{-h_m-h(x,y)/2}^{-h(x,y)/2}\underline{C}_{44}(1,z,z^2)dz+\int_{-h(x,y)/2}^{h(x,y)/2}Q_{44}(z)(1,z,z^2)dz+\int_{h(x,y)/2}^{h(x,y)/2+h_m}\underline{C}_{44}(1,z,z^2)dz,$$

$$(A_{66},B_{66},H_{66})=\int_{-h_m-h(x,y)/2}^{-h(x,y)/2}\underline{C}_{66}(1,z,z^2)dz+\int_{-h(x,y)/2}^{h(x,y)/2}Q_{66}(z)(1,z,z^2)dz+\int_{h(x,y)/2}^{h(x,y)/2+h_m}\underline{C}_{66}(1,z,z^2)dz,$$

$$F_{31}=\int_{-h_m-h(x,y)/2}^{-h(x,y)/2}\underline{e}_{31}\frac{\pi}{h_m}sin\left\{\frac{\pi\left[z+\left(\frac{h(x,y)+h_m}{2}\right)\right]}{h_m}\right\}dz+\int_{h(x,y)/2}^{h(x,y)/2+h_m}\underline{e}_{31}\frac{\pi}{h_m}sin\left\{\frac{\pi\left[z-\left(\frac{h(x,y)+h_m}{2}\right)\right]}{h_m}\right\}dz,$$

$$\bar{F}_{31}=\int_{-h_m-h(x,y)/2}^{-h(x,y)/2}\underline{e}_{31}\frac{\pi}{h_m}sin\left\{\frac{\pi\left[z+\left(\frac{h(x,y)+h_m}{2}\right)\right]}{h_m}\right\}zdz+\int_{h(x,y)/2}^{h(x,y)/2+h_m}\underline{e}_{31}\frac{\pi}{h_m}sin\left\{\frac{\pi\left[z-\left(\frac{h(x,y)+h_m}{2}\right)\right]}{h_m}\right\}zdz,$$

$$F_{15}=\int_{-h_m-h(x,y)/2}^{-h(x,y)/2}\underline{e}_{15}cos\left\{\frac{\pi\left[z+\left(\frac{h(x,y)+h_m}{2}\right)\right]}{h_m}\right\}dz+\int_{h(x,y)/2}^{h(x,y)/2+h_m}\underline{e}_{15}cos\left\{\frac{\pi\left[z-\left(\frac{h(x,y)+h_m}{2}\right)\right]}{h_m}\right\}dz,$$

$$\bar{F}_{15}=\int_{-h_m-h(x,y)/2}^{-h(x,y)/2}\underline{e}_{15}\frac{\pi}{2h_m}\frac{\partial h(x,y)}{\partial x}sin\left\{\frac{\pi\left[z+\left(\frac{h(x,y)+h_m}{2}\right)\right]}{h_m}\right\}dz+\int_{h(x,y)/2}^{h(x,y)/2+h_m}\underline{e}_{15}\frac{\pi}{2h_m}\frac{\partial h(x,y)}{\partial x}sin\left\{\frac{\pi\left[z-\left(\frac{h(x,y)+h_m}{2}\right)\right]}{h_m}\right\}dz,$$

$$F_{24}=\int_{-h_m-h(x,y)/2}^{-h(x,y)/2}\underline{e}_{24}cos\left\{\frac{\pi\left[z+\left(\frac{h(x,y)+h_m}{2}\right)\right]}{h_m}\right\}dz+\int_{h(x,y)/2}^{h(x,y)/2+h_m}\underline{e}_{24}cos\left\{\frac{\pi\left[z-\left(\frac{h(x,y)+h_m}{2}\right)\right]}{h_m}\right\}dz,$$

$$\bar{F}_{24}=\int_{-h_m-h(x,y)/2}^{-h(x,y)/2}\underline{e}_{24}\frac{\pi}{2h_m}\frac{\partial h(x,y)}{\partial x}sin\left\{\frac{\pi\left[z+\left(\frac{h(x,y)+h_m}{2}\right)\right]}{h_m}\right\}dz+\int_{h(x,y)/2}^{h(x,y)/2+h_m}\underline{e}_{24}\frac{\pi}{2h_m}\frac{\partial h(x,y)}{\partial x}sin\left\{\frac{\pi\left[z-\left(\frac{h(x,y)+h_m}{2}\right)\right]}{h_m}\right\}dz,$$

$$F_{16} = \int_{-h_m-h(x,y)/2}^{-h(x,y)/2} \underline{e}_{15} \frac{\pi}{2h_m} \frac{\partial h(x,y)}{\partial x} sin\left\{\frac{\pi\left[z+\left(\frac{h(x,y)+h_m}{2}\right)\right]}{h_m}\right\} dz + \int_{h(x,y)/2}^{h(x,y)/2+h_m} \underline{e}_{15} \frac{\pi}{2h_m} \frac{\partial h(x,y)}{\partial x} sin\left\{\frac{\pi\left[z-\left(\frac{h(x,y)+h_m}{2}\right)\right]}{h_m}\right\} dz ,$$

$$F_{26} = \int_{-h_m-h(x,y)/2}^{-h(x,y)/2} \underline{e}_{24} \frac{\pi}{2h_m} \frac{\partial h(x,y)}{\partial x} sin\left\{\frac{\pi\left[z+\left(\frac{h(x,y)+h_m}{2}\right)\right]}{h_m}\right\} dz + \int_{h(x,y)/2}^{h(x,y)/2+h_m} \underline{e}_{24} \frac{\pi}{2h_m} \frac{\partial h(x,y)}{\partial x} sin\left\{\frac{\pi\left[z-\left(\frac{h(x,y)+h_m}{2}\right)\right]}{h_m}\right\} dz ,$$

$$F_1 = \int_{-h_m-h(x,y)/2}^{-h(x,y)/2} \frac{1}{4} \underline{k}_{11} \left(\frac{\pi}{h_m}\right)^2 \left(\frac{\partial h(x,y)}{\partial x}\right)^2 sin^2\left\{\frac{\pi\left[z+\left(\frac{h(x,y)+h_m}{2}\right)\right]}{h_m}\right\} \int_{h(x,y)/2}^{h(x,y)/2+h_m} \frac{1}{4} \underline{k}_{11} \left(\frac{\pi}{h_m}\right)^2 \left(\frac{\partial h(x,y)}{\partial x}\right)^2 sin^2\left\{\frac{\pi\left[z-\left(\frac{h(x,y)+h_m}{2}\right)\right]}{h_m}\right\}$$

,

$$\bar{F}_1 = \int_{-h_m-h(x,y)/2}^{-h(x,y)/2} \frac{1}{4} \underline{k}_{22} \left(\frac{\pi}{h_m}\right)^2 \left(\frac{\partial h(x,y)}{\partial x}\right)^2 sin^2\left\{\frac{\pi\left[z+\left(\frac{h(x,y)+h_m}{2}\right)\right]}{h_m}\right\} \int_{h(x,y)/2}^{h(x,y)/2+h_m} \frac{1}{4} \underline{k}_{22} \left(\frac{\pi}{h_m}\right)^2 \left(\frac{\partial h(x,y)}{\partial x}\right)^2 sin^2\left\{\frac{\pi\left[z-\left(\frac{h(x,y)+h_m}{2}\right)\right]}{h_m}\right\}$$

,

$$F_2 = \int_{-h_m-h(x,y)/2}^{-h(x,y)/2} \frac{1}{2} \underline{k}_{11} \left(\frac{\pi}{h_m}\right) \left(\frac{\partial^2 h(x,y)}{\partial x^2}\right) sin\left\{\frac{\pi\left[z+\left(\frac{h(x,y)+h_m}{2}\right)\right]}{h_m}\right\} co \int_{h(x,y)/2}^{h(x,y)/2+h_m} \frac{1}{2} \underline{k}_{11} \left(\frac{\pi}{h_m}\right) \left(\frac{\partial^2 h(x,y)}{\partial x^2}\right) sin\left\{\frac{\pi\left[z-\left(\frac{h(x,y)+h_m}{2}\right)\right]}{h_m}\right\} co.$$

,

$$\bar{F}_2 = \int_{-h_m-h(x,y)/2}^{-h(x,y)/2} \frac{1}{2} \underline{k}_{22} \left(\frac{\pi}{h_m}\right) \left(\frac{\partial^2 h(x,y)}{\partial x^2}\right) sin\left\{\frac{\pi\left[z+\left(\frac{h(x,y)+h_m}{2}\right)\right]}{h_m}\right\} co \int_{h(x,y)/2}^{h(x,y)/2+h_m} \frac{1}{2} \underline{k}_{22} \left(\frac{\pi}{h_m}\right) \left(\frac{\partial^2 h(x,y)}{\partial x^2}\right) sin\left\{\frac{\pi\left[z-\left(\frac{h(x,y)+h_m}{2}\right)\right]}{h_m}\right\} co.$$

,

$$F_3 = \int_{-h_m-h(x,y)/2}^{-h(x,y)/2} \frac{1}{4} \underline{k}_{11} \left(\frac{\pi}{h_m}\right)^2 \left(\frac{\partial h(x,y)}{\partial x}\right)^2 cos^2\left\{\frac{\pi\left[z+\left(\frac{h(x,y)+h_m}{2}\right)\right]}{h_m}\right\} \int_{h(x,y)/2}^{h(x,y)/2+h_m} \frac{1}{4} \underline{k}_{11} \left(\frac{\pi}{h_m}\right)^2 \left(\frac{\partial h(x,y)}{\partial x}\right)^2 cos^2\left\{\frac{\pi\left[z-\left(\frac{h(x,y)+h_m}{2}\right)\right]}{h_m}\right\}$$

,

$$\bar{F}_3 = \int_{-h_m-h(x,y)/2}^{-h(x,y)/2} \frac{1}{4} \underline{k}_{22} \left(\frac{\pi}{h_m}\right)^2 \left(\frac{\partial h(x,y)}{\partial x}\right)^2 cos^2\left\{\frac{\pi\left[z+\left(\frac{h(x,y)+h_m}{2}\right)\right]}{h_m}\right\} \int_{h(x,y)/2}^{h(x,y)/2+h_m} \frac{1}{4} \underline{k}_{22} \left(\frac{\pi}{h_m}\right)^2 \left(\frac{\partial h(x,y)}{\partial x}\right)^2 cos^2\left\{\frac{\pi\left[z-\left(\frac{h(x,y)+h_m}{2}\right)\right]}{h_m}\right\}$$

,

$$F_4 = \int_{-h_m-h(x,y)/2}^{-h(x,y)/2} \frac{3}{2} \underline{k}_{11} \left(\frac{\pi}{h_m}\right) \left(\frac{\partial h(x,y)}{\partial x}\right) sin\left\{\frac{\pi\left[z+\left(\frac{h(x,y)+h_m}{2}\right)\right]}{h_m}\right\} cos \int_{h(x,y)/2}^{h(x,y)/2+h_m} \frac{3}{2} \underline{k}_{11} \left(\frac{\pi}{h_m}\right) \left(\frac{\partial h(x,y)}{\partial x}\right) sin\left\{\frac{\pi\left[z-\left(\frac{h(x,y)+h_m}{2}\right)\right]}{h_m}\right\} cos$$

,

$$\bar{F}_4 = \int_{-h_m-h(x,y)/2}^{-h(x,y)/2} \frac{3}{2} \underline{k}_{22} \left(\frac{\pi}{h_m}\right) \left(\frac{\partial h(x,y)}{\partial x}\right) sin\left\{\frac{\pi\left[z+\left(\frac{h(x,y)+h_m}{2}\right)\right]}{h_m}\right\} cos \int_{h(x,y)/2}^{h(x,y)/2+h_m} \frac{3}{2} \underline{k}_{22} \left(\frac{\pi}{h_m}\right) \left(\frac{\partial h(x,y)}{\partial x}\right) sin\left\{\frac{\pi\left[z-\left(\frac{h(x,y)+h_m}{2}\right)\right]}{h_m}\right\} cos$$

,

$$F_5 = \int_{-h_m-h(x,y)/2}^{-h(x,y)/2} \underline{k}_{11} cos^2\left\{\frac{\pi\left[z+\left(\frac{h(x,y)+h_m}{2}\right)\right]}{h_m}\right\} dz + \int_{h(x,y)/2}^{h(x,y)/2+h_m} \underline{k}_{11} cos^2\left\{\frac{\pi\left[z-\left(\frac{h(x,y)+h_m}{2}\right)\right]}{h_m}\right\} dz ,$$

$$\bar{F}_5 = \int_{-h_m-h(x,y)/2}^{-h(x,y)/2} \underline{k}_{22} cos^2\left\{\frac{\pi\left[z+\left(\frac{h(x,y)+h_m}{2}\right)\right]}{h_m}\right\} dz + \int_{h(x,y)/2}^{h(x,y)/2+h_m} \underline{k}_{22} cos^2\left\{\frac{\pi\left[z-\left(\frac{h(x,y)+h_m}{2}\right)\right]}{h_m}\right\} dz ,$$

$$F_6 = \int_{-h_m-h(x,y)/2}^{-h(x,y)/2} \frac{1}{4} \underline{a}_{11} \left(\frac{\pi}{h_m}\right)^2 \left(\frac{\partial h(x,y)}{\partial x}\right)^2 sin^2\left\{\frac{\pi\left[z+\left(\frac{h(x,y)+h_m}{2}\right)\right]}{h_m}\right\} \int_{h(x,y)/2}^{h(x,y)/2+h_m} \frac{1}{4} \underline{a}_{11} \left(\frac{\pi}{h_m}\right)^2 \left(\frac{\partial h(x,y)}{\partial x}\right)^2 sin^2\left\{\frac{\pi\left[z-\left(\frac{h(x,y)+h_m}{2}\right)\right]}{h_m}\right\}$$

,

$$\bar{F}_6 = \int_{-h_m-h(x,y)/2}^{-h(x,y)/2} \frac{1}{4} \underline{a}_{22} \left(\frac{\pi}{h_m}\right)^2 \left(\frac{\partial h(x,y)}{\partial x}\right)^2 sin^2\left\{\frac{\pi\left[z+\left(\frac{h(x,y)+h_m}{2}\right)\right]}{h_m}\right\} \int_{h(x,y)/2}^{h(x,y)/2+h_m} \frac{1}{4} \underline{a}_{22} \left(\frac{\pi}{h_m}\right)^2 \left(\frac{\partial h(x,y)}{\partial x}\right)^2 sin^2\left\{\frac{\pi\left[z-\left(\frac{h(x,y)+h_m}{2}\right)\right]}{h_m}\right\}$$

,

$$F_7 = \int_{-h_m-h(x,y)/2}^{-h(x,y)/2} \frac{1}{2} \underline{a}_{11} \left(\frac{\pi}{h_m}\right) \left(\frac{\partial^2 h(x,y)}{\partial x^2}\right) sin\left\{\frac{\pi\left[z+\left(\frac{h(x,y)+h_m}{2}\right)\right]}{h_m}\right\} co \int_{h(x,y)/2}^{h(x,y)/2+h_m} \frac{1}{2} \underline{a}_{11} \left(\frac{\pi}{h_m}\right) \left(\frac{\partial^2 h(x,y)}{\partial x^2}\right) sin\left\{\frac{\pi\left[z-\left(\frac{h(x,y)+h_m}{2}\right)\right]}{h_m}\right\} co.$$

,

$$\bar{F}_7 = \int_{-h_m-h(x,y)/2}^{-h(x,y)/2} \frac{1}{2} \underline{a}_{22} \left(\frac{\pi}{h_m}\right) \left(\frac{\partial^2 h(x,y)}{\partial x^2}\right) sin\left\{\frac{\pi\left[z+\left(\frac{h(x,y)+h_m}{2}\right)\right]}{h_m}\right\} co \int_{h(x,y)/2}^{h(x,y)/2+h_m} \frac{1}{2} \underline{a}_{22} \left(\frac{\pi}{h_m}\right) \left(\frac{\partial^2 h(x,y)}{\partial x^2}\right) sin\left\{\frac{\pi\left[z-\left(\frac{h(x,y)+h_m}{2}\right)\right]}{h_m}\right\} co.$$

,

$$F_8 = \int_{-h_m-h(x,y)/2}^{-h(x,y)/2} \frac{1}{4} \underline{a}_{11} \left(\frac{\pi}{h_m}\right)^2 \left(\frac{\partial h(x,y)}{\partial x}\right)^2 cos^2\left\{\frac{\pi\left[z+\left(\frac{h(x,y)+h_m}{2}\right)\right]}{h_m}\right\} \int_{h(x,y)/2}^{h(x,y)/2+h_m} \frac{1}{4} \underline{a}_{11} \left(\frac{\pi}{h_m}\right)^2 \left(\frac{\partial h(x,y)}{\partial x}\right)^2 cos^2\left\{\frac{\pi\left[z-\left(\frac{h(x,y)+h_m}{2}\right)\right]}{h_m}\right\}$$

,

$$\bar{F}_8 = \int_{-h_m-h(x,y)/2}^{-h(x,y)/2} \frac{1}{4} \underline{a}_{22} \left(\frac{\pi}{h_m}\right)^2 \left(\frac{\partial h(x,y)}{\partial x}\right)^2 cos^2\left\{\frac{\pi\left[z+\left(\frac{h(x,y)+h_m}{2}\right)\right]}{h_m}\right\} \int_{h(x,y)/2}^{h(x,y)/2+h_m} \frac{1}{4} \underline{a}_{22} \left(\frac{\pi}{h_m}\right)^2 \left(\frac{\partial h(x,y)}{\partial x}\right)^2 cos^2\left\{\frac{\pi\left[z-\left(\frac{h(x,y)+h_m}{2}\right)\right]}{h_m}\right\}$$

,

$$F_9 = \int_{-h_m-h(x,y)/2}^{-h(x,y)/2} \frac{3}{2}\underline{a}_{11}\left(\frac{\pi}{h_m}\right)\left(\frac{\partial h(x,y)}{\partial x}\right) sin\left\{\frac{\pi\left[z+\left(\frac{h(x,y)+h_m}{2}\right)\right]}{h_m}\right\} cos$$
$$\int_{h(x,y)/2}^{h(x,y)/2+h_m} \frac{3}{2}\underline{a}_{11}\left(\frac{\pi}{h_m}\right)\left(\frac{\partial h(x,y)}{\partial x}\right) sin\left\{\frac{\pi\left[z-\left(\frac{h(x,y)+h_m}{2}\right)\right]}{h_m}\right\} cos$$

,

$$\bar{F}_9 = \int_{-h_m-h(x,y)/2}^{-h(x,y)/2} \frac{3}{2}\underline{a}_{22}\left(\frac{\pi}{h_m}\right)\left(\frac{\partial h(x,y)}{\partial x}\right) sin\left\{\frac{\pi\left[z+\left(\frac{h(x,y)+h_m}{2}\right)\right]}{h_m}\right\} cos$$
$$\int_{h(x,y)/2}^{h(x,y)/2+h_m} \frac{3}{2}\underline{a}_{22}\left(\frac{\pi}{h_m}\right)\left(\frac{\partial h(x,y)}{\partial x}\right) sin\left\{\frac{\pi\left[z-\left(\frac{h(x,y)+h_m}{2}\right)\right]}{h_m}\right\} cos$$

,

$$F_{10} = \int_{-h_m-h(x,y)/2}^{-h(x,y)/2} \underline{a}_{11} cos^2\left\{\frac{\pi\left[z+\left(\frac{h(x,y)+h_m}{2}\right)\right]}{h_m}\right\} dz +$$
$$\int_{h(x,y)/2}^{h(x,y)/2+h_m} \underline{a}_{11} cos^2\left\{\frac{\pi\left[z-\left(\frac{h(x,y)+h_m}{2}\right)\right]}{h_m}\right\} dz\,,$$

$$\bar{F}_{10} = \int_{-h_m-h(x,y)/2}^{-h(x,y)/2} \underline{a}_{22} cos^2\left\{\frac{\pi\left[z+\left(\frac{h(x,y)+h_m}{2}\right)\right]}{h_m}\right\} dz +$$
$$\int_{h(x,y)/2}^{h(x,y)/2+h_m} \underline{a}_{22} cos^2\left\{\frac{\pi\left[z-\left(\frac{h(x,y)+h_m}{2}\right)\right]}{h_m}\right\} dz\,,$$

$$F_{33} = \int_{-h_m-h(x,y)/2}^{-h(x,y)/2} \underline{k}_{33}\left(\frac{\pi}{h_m}\right)^2 sin^2\left\{\frac{\pi\left[z+\left(\frac{h(x,y)+h_m}{2}\right)\right]}{h_m}\right\} dz +$$
$$\int_{h(x,y)/2}^{h(x,y)/2+h_m} \underline{k}_{33}\left(\frac{\pi}{h_m}\right)^2 sin^2\left\{\frac{\pi\left[z-\left(\frac{h(x,y)+h_m}{2}\right)\right]}{h_m}\right\} dz\,,$$

$$G_{31} = \int_{-h_m-h(x,y)/2}^{-h(x,y)/2} \underline{q}_{31}\frac{\pi}{h_m} sin\left\{\frac{\pi\left[z+\left(\frac{h(x,y)+h_m}{2}\right)\right]}{h_m}\right\} dz +$$
$$\int_{h/2}^{h/2+h_m} \underline{q}_{31}\frac{\pi}{h_m} sin\left\{\frac{\pi\left[z-\left(\frac{h(x,y)+h_m}{2}\right)\right]}{h_m}\right\} dz,$$

$$\bar{G}_{31} = \int_{-h_m-h(x,y)/2}^{-h(x,y)/2} \underline{q}_{31}\frac{\pi}{h_m} sin\left\{\frac{\pi\left[z+\left(\frac{h(x,y)+h_m}{2}\right)\right]}{h_m}\right\} zdz +$$
$$\int_{h/2}^{h/2+h_m} \underline{q}_{31}\frac{\pi}{h_m} sin\left\{\frac{\pi\left[z-\left(\frac{h(x,y)+h_m}{2}\right)\right]}{h_m}\right\} zdz,$$

$$G_{16} = \int_{-h_m-h(x,y)/2}^{-h(x,y)/2} \underline{q}_{15}\frac{\pi}{2h_m}\frac{\partial h(x,y)}{\partial x} sin\left\{\frac{\pi\left[z+\left(\frac{h(x,y)+h_m}{2}\right)\right]}{h_m}\right\} dz +$$
$$\int_{h(x,y)/2}^{h(x,y)/2+h_m} \underline{q}_{15}\frac{\pi}{2h_m}\frac{\partial h(x,y)}{\partial x} sin\left\{\frac{\pi\left[z-\left(\frac{h(x,y)+h_m}{2}\right)\right]}{h_m}\right\} dz\,,$$

$$G_{26} = \int_{-h_m-h(x,y)/2}^{-h(x,y)/2} \underline{q}_{24}\frac{\pi}{2h_m}\frac{\partial h(x,y)}{\partial x} sin\left\{\frac{\pi\left[z+\left(\frac{h(x,y)+h_m}{2}\right)\right]}{h_m}\right\} dz +$$
$$\int_{h(x,y)/2}^{h(x,y)/2+h_m} q_{24}\frac{\pi}{2h_m}\frac{\partial h(x,y)}{\partial x} sin\left\{\frac{\pi\left[z-\left(\frac{h(x,y)+h_m}{2}\right)\right]}{h_m}\right\} dz\,,$$

$$G_{33} = \int_{-h_m-h(x,y)/2}^{-h(x,y)/2} \underline{a}_{33}\left(\frac{\pi}{h_m}\right)^2 sin^2\left\{\frac{\pi\left[z+\left(\frac{h(x,y)+h_m}{2}\right)\right]}{h_m}\right\} dz +$$
$$\int_{h(x,y)/2}^{h(x,y)/2+h_m} \underline{a}_{33}\left(\frac{\pi}{h_m}\right)^2 sin^2\left\{\frac{\pi\left[z-\left(\frac{h(x,y)+h_m}{2}\right)\right]}{h_m}\right\} dz$$

$$G_{15} = \int_{-h_m-\frac{h(x,y)}{2}}^{-\frac{h(x,y)}{2}} \underline{q}_{15} cos\left\{\frac{\pi\left[z+\left(\frac{h(x,y)+h_m}{2}\right)\right]}{h_m}\right\} dz +$$
$$\int_{\frac{h(x,y)}{2}}^{\frac{h(x,y)}{2}+h_m} \underline{q}_{31} cos\left\{\frac{\pi\left[z-\left(\frac{h(x,y)+h_m}{2}\right)\right]}{h_m}\right\} dz,$$

$$\bar{G}_{15} = \int_{-h_m-h(x,y)/2}^{-h(x,y)/2} \underline{q}_{15}\frac{\pi}{2h_m}\frac{\partial h(x,y)}{\partial x} sin\left\{\frac{\pi\left[z+\left(\frac{h(x,y)+h_m}{2}\right)\right]}{h_m}\right\} dz +$$
$$\int_{h(x,y)/2}^{h(x,y)/2+h_m} \underline{q}_{15}\frac{\pi}{2h_m}\frac{\partial h(x,y)}{\partial x} sin\left\{\frac{\pi\left[z-\left(\frac{h(x,y)+h_m}{2}\right)\right]}{h_m}\right\} dz$$

$$G_{24} = \int_{-h_m-h(x,y)/2}^{-h(x,y)/2} \underline{q}_{24} cos\left\{\frac{\pi\left[z+\left(\frac{h(x,y)+h_m}{2}\right)\right]}{h_m}\right\} dz +$$
$$\int_{h(x,y)/2}^{h(x,y)/2+h_m} \underline{q}_{24} cos\left\{\frac{\pi\left[z-\left(\frac{h(x,y)+h_m}{2}\right)\right]}{h_m}\right\} dz,$$

$$\bar{G}_{24} = \int_{-h_m-h(x,y)/2}^{-h(x,y)/2} \underline{q}_{24}\frac{\pi}{2h_m}\frac{\partial h(x,y)}{\partial x} sin\left\{\frac{\pi\left[z+\left(\frac{h(x,y)+h_m}{2}\right)\right]}{h_m}\right\} dz +$$
$$\int_{h(x,y)/2}^{h(x,y)/2+h_m} \underline{q}_{24}\frac{\pi}{2h_m}\frac{\partial h(x,y)}{\partial x} sin\left\{\frac{\pi\left[z-\left(\frac{h(x,y)+h_m}{2}\right)\right]}{h_m}\right\} dz\,,$$

$$F_{11} = \int_{-h_m-h(x,y)/2}^{-h(x,y)/2} \frac{1}{4}\underline{\mu}_{11}\left(\frac{\pi}{h_m}\right)^2\left(\frac{\partial h(x,y)}{\partial x}\right)^2 sin^2\left\{\frac{\pi\left[z+\left(\frac{h(x,y)+h_m}{2}\right)\right]}{h_m}\right\}$$
$$\int_{h(x,y)/2}^{h(x,y)/2+h_m} \frac{1}{4}\underline{\mu}_{11}\left(\frac{\pi}{h_m}\right)^2\left(\frac{\partial h(x,y)}{\partial x}\right)^2 sin^2\left\{\frac{\pi\left[z-\left(\frac{h(x,y)+h_m}{2}\right)\right]}{h_m}\right\}$$

,

$$\bar{F}_{11} = \int_{-h_m-h(x,y)/2}^{-h(x,y)/2} \frac{1}{4}\underline{\mu}_{22}\left(\frac{\pi}{h_m}\right)^2\left(\frac{\partial h(x,y)}{\partial x}\right)^2 sin^2\left\{\frac{\pi\left[z+\left(\frac{h(x,y)+h_m}{2}\right)\right]}{h_m}\right\}$$
$$\int_{h(x,y)/2}^{h(x,y)/2+h_m} \frac{1}{4}\underline{\mu}_{22}\left(\frac{\pi}{h_m}\right)^2\left(\frac{\partial h(x,y)}{\partial x}\right)^2 sin^2\left\{\frac{\pi\left[z-\left(\frac{h(x,y)+h_m}{2}\right)\right]}{h_m}\right\}$$

,

$$F_{12} = \int_{-h_m-h(x,y)/2}^{-h(x,y)/2} \frac{1}{2}\underline{\mu}_{11}\left(\frac{\pi}{h_m}\right)\left(\frac{\partial^2 h(x,y)}{\partial x^2}\right) sin\left\{\frac{\pi\left[z+\left(\frac{h(x,y)+h_m}{2}\right)\right]}{h_m}\right\}$$
$$\int_{h(x,y)/2}^{h(x,y)/2+h_m} \frac{1}{2}\underline{\mu}_{11}\left(\frac{\pi}{h_m}\right)\left(\frac{\partial^2 h(x,y)}{\partial x^2}\right) sin\left\{\frac{\pi\left[z-\left(\frac{h(x,y)+h_m}{2}\right)\right]}{h_m}\right\}$$

,

$$\bar{F}_{12} = \int_{-h_m-h(x,y)/2}^{-h(x,y)/2} \frac{1}{2}\underline{\mu}_{22}\left(\frac{\pi}{h_m}\right)\left(\frac{\partial^2 h(x,y)}{\partial x^2}\right) sin\left\{\frac{\pi\left[z+\left(\frac{h(x,y)+h_m}{2}\right)\right]}{h_m}\right\}$$
$$\int_{h(x,y)/2}^{h(x,y)/2+h_m} \frac{1}{2}\underline{\mu}_{22}\left(\frac{\pi}{h_m}\right)\left(\frac{\partial^2 h(x,y)}{\partial x^2}\right) sin\left\{\frac{\pi\left[z-\left(\frac{h(x,y)+h_m}{2}\right)\right]}{h_m}\right\}$$

,

$$F_{13} = \int_{-h_m-h(x,y)/2}^{-h(x,y)/2} \frac{1}{4}\underline{\mu}_{11}\left(\frac{\pi}{h_m}\right)^2\left(\frac{\partial h(x,y)}{\partial x}\right)^2 cos^2\left\{\frac{\pi\left[z+\left(\frac{h(x,y)+h_m}{2}\right)\right]}{h_m}\right\}$$
$$\int_{h(x,y)/2}^{h(x,y)/2+h_m} \frac{1}{4}\underline{\mu}_{11}\left(\frac{\pi}{h_m}\right)^2\left(\frac{\partial h(x,y)}{\partial x}\right)^2 cos^2\left\{\frac{\pi\left[z-\left(\frac{h(x,y)+h_m}{2}\right)\right]}{h_m}\right\}$$

,

$$\bar{F}_{13} = \int_{-h_m-h(x,y)/2}^{-h(x,y)/2} \frac{1}{4}\underline{\mu}_{22}\left(\frac{\pi}{h_m}\right)^2\left(\frac{\partial h(x,y)}{\partial x}\right)^2 cos^2\left\{\frac{\pi\left[z+\left(\frac{h(x,y)+h_m}{2}\right)\right]}{h_m}\right\} \int_{h(x,y)/2}^{h(x,y)/2+h_m} \frac{1}{4}\underline{\mu}_{22}\left(\frac{\pi}{h_m}\right)^2\left(\frac{\partial h(x,y)}{\partial x}\right)^2 cos^2\left\{\frac{\pi\left[z-\left(\frac{h(x,y)+h_m}{2}\right)\right]}{h_m}\right\}$$

,

$$F_{14} = \int_{-h_m-h(x,y)/2}^{-h(x,y)/2} \frac{3}{2}\underline{\mu}_{11}\left(\frac{\pi}{h_m}\right)\left(\frac{\partial h(x,y)}{\partial x}\right) sin\left\{\frac{\pi\left[z+\left(\frac{h(x,y)+h_m}{2}\right)\right]}{h_m}\right\} cos \int_{h(x,y)/2}^{h(x,y)/2+h_m} \frac{3}{2}\underline{\mu}_{11}\left(\frac{\pi}{h_m}\right)\left(\frac{\partial h(x,y)}{\partial x}\right) sin\left\{\frac{\pi\left[z-\left(\frac{h(x,y)+h_m}{2}\right)\right]}{h_m}\right\} cos$$

,

$$\bar{F}_{14} = \int_{-h_m-h(x,y)/2}^{-h(x,y)/2} \frac{3}{2}\mu_{22}\left(\frac{\pi}{h_m}\right)\left(\frac{\partial h(x,y)}{\partial x}\right) sin\left\{\frac{\pi\left[z+\left(\frac{h(x,y)+h_m}{2}\right)\right]}{h_m}\right\} cos \int_{h(x,y)/2}^{h(x,y)/2+h_m} \frac{3}{2}\mu_{22}\left(\frac{\pi}{h_m}\right)\left(\frac{\partial h(x,y)}{\partial x}\right) sin\left\{\frac{\pi\left[z-\left(\frac{h(x,y)+h_m}{2}\right)\right]}{h_m}\right\} cos$$

,

$$F_{15} = \int_{-h_m-h(x,y)/2}^{-h(x,y)/2} \underline{\mu}_{11} cos^2\left\{\frac{\pi\left[z+\left(\frac{h(x,y)+h_m}{2}\right)\right]}{h_m}\right\} dz + \int_{h(x,y)/2}^{h(x,y)/2+h_m} \mu_{11} cos^2\left\{\frac{\pi\left[z-\left(\frac{h(x,y)+h_m}{2}\right)\right]}{h_m}\right\} dz ,$$

$$\bar{F}_{15} = \int_{-h_m-h(x,y)/2}^{-h(x,y)/2} \underline{\mu}_{22} cos^2\left\{\frac{\pi\left[z+\left(\frac{h(x,y)+h_m}{2}\right)\right]}{h_m}\right\} dz + \int_{h(x,y)/2}^{h(x,y)/2+h_m} \underline{\mu}_{22} cos^2\left\{\frac{\pi\left[z-\left(\frac{h(x,y)+h_m}{2}\right)\right]}{h_m}\right\} dz ,$$

$$P_{33} = \int_{-h_m-h(x,y)/2}^{-h(x,y)/2} \underline{\mu}_{33}\left(\frac{\pi}{h_m}\right)^2 sin^2\left\{\frac{\pi\left[z+\left(\frac{h(x,y)+h_m}{2}\right)\right]}{h_m}\right\} dz + \int_{h(x,y)/2}^{h(x,y)/2+h_m} \mu_{33}\left(\frac{\pi}{h_m}\right)^2 sin^2\left\{\frac{\pi\left[z-\left(\frac{h(x,y)+h_m}{2}\right)\right]}{h_m}\right\} dz$$

References

[1] A. R. Saidi, M. Abdollahi, R. Bahaadini, Flutter analysis of honeycomb sandwich trapezoidal wings reinforced with GPLs, *Thin-Walled Structures*, 2023, **183**, 110353, doi: 10.1016/j.tws.2022.110353.

[2] S. Pourhemmati, S. Hossainpour, Thermal improvement of the vertical plate-fin heat sink by variable fin thickness pattern and utilizing phase change material: a numerical investigation, *Journal of Energy Storage*, 2023, **59**, 106480, doi: 10.1016/j.est.2022.106480.

[3] P. Roodgar Saffari, W. Sher, C. Thongchom, Size dependent buckling analysis of a FG-CNTRC microplate of variable thickness under non-uniform biaxial compression, *Buildings*, 2022, **12**, 2238, doi: 10.3390/buildings12122238.

[4] H. N. Thi, Thermal vibration analysis of functionally graded porous plates with variable thickness resting on elastic foundations using finite element method, *Mechanics Based Design of Structures and Machines*, 2022, 1-29, doi: 10.1080/15397734.2022.2047719.

[5] N. Ahlawat, R. Saini, Vibration and buckling analysis of elastically supported Bi-directional FGM mindlin circular plates having variable thickness, *Journal of Vibration Engineering & Technologies*, 2023, 1-20, doi: 10.1007/s42417-023-00856-1.

[6] D. Chen, S. Kitipornchai, J. Yang, Dynamic response and energy absorption of functionally graded porous structures, *Materials & Design*, 2018, **140**, 473-487, doi: 10.1016/j.matdes.2017.12.019.

[7] J. Wang, A. Liu, Q. Ao, C. Wu, J. Ma, P. Cao, Energy absorption characteristics and preparation of porous titanium with high porosity, *Materials Today Communications*, 2023, **34**, 105003, doi: 10.1016/j.mtcomm.2022.105003.

[8] X. Meng, S. Tan, Z. Yuan, Y. Zhang, L. Chen, Experimental study on the heat transfer performance of a vapour chamber with porous wick structures printed via metallic additive manufacturing, *International Communications in Heat and Mass Transfer*, 2023, **140**, 106496, doi: 10.1016/j.icheatmasstransfer.2022.106496.

[9] J. Zhou, A. Bhaskar, X. Zhang, The effect of external mean flow on sound transmission through double-walled cylindrical shells lined with poroelastic material, *Journal of Sound and Vibration*, 2014, **333**, 1972–1990, doi: 10.1016/j.jsv.2013.11.038.

[10] D. Chen, J. Yang, S. Kitipornchai, Free and forced vibrations of shear deformable functionally graded porous beams, *International Journal of Mechanical Sciences*, 2016, **108-109**, 14-22, doi: 10.1016/j.ijmecsci.2016.01.025.

[11] T. Q. Hung, D. M. Duc, T. M. Tu, Free and forced vibration characteristics of functionally graded sandwich beam with GPL-reinforced porous core. Lecture Notes in Civil Engineering. Singapore: Springer Nature Singapore, 2023: 1432-1452, doi: 10.1007/978-981-19-7331-4_114.

[12] Y. Q. Wang, J. W. Zu, Porosity-dependent nonlinear forced vibration analysis of functionally graded piezoelectric smart material plates, *Smart Materials and Structures*, 2017, **26**, 105014, doi: 10.1088/1361-665x/aa8429.

[13] Xiao, Yushan, A novel Gaussian higher-order plate theory for dynamic response of porous sandwich plates with different geometries, *Thin-Walled Structures*, 2023, **185**, 110599, doi: 10.1016/j.tws.2023.110599.

[14] F. Ebrahimi, D. Hashemabadi, M. Habibi, H. Safarpour, Thermal buckling and forced vibration characteristics of a porous GNP reinforced nanocomposite cylindrical shell, *Microsystem Technologies*, 2020, **26**, 461-473, doi: 10.1007/s00542-019-04542-9.

[15] G. Pourmoosavi, S. A. M. Ghasemi, B. F. Azar, S. Talatahari, Shear design curves of unstiffened plate girder web panels at high temperatures, *Journal of Constructional Steel Research*, 2020, **164**, 105808, doi: 10.1016/j.jcsr.2019.105808.

[16] G. H. Pourmoosavi, S. A. Mousavi Ghasemi, B. Farahmand Azar, S. Talatahari, Numerical investigation on ultimate shear strength of long steel plate girder web panels at high temperatures, *Journal of Building Engineering*, 2020, **29**, 101070, doi: 10.1016/j.jobe.2019.101070.

[17] Y. H. Song, E. K. Ji, B. W. Jeong, M. K. Jung, E. Y. Kim, D.

H. Yoon, High power laser-driven ceramic phosphor plate for outstanding efficient white light conversion in application of automotive lighting, *Scientific Reports*, 2016, **6**, 31206, doi: 10.1038/srep31206.
[18] L. Yang, Y. Guo, B. Shi, C. Kuang, W. Xu, S. Cao, Study of scour around submarine pipeline with a rubber plate or rigid spoiler in wave conditions, *Journal of Waterway, Port, Coastal, and Ocean Engineering*, 2012, **138**, 484-490, doi: 10.1061/(asce)ww.1943-5460.0000150.
[19] Y. Xue, G. Jin, X. Ma, H. Chen, T. Ye, M. Chen, Y. Zhang, Free vibration analysis of porous plates with porosity distributions in the thickness and in-plane directions using isogeometric approach, *International Journal of Mechanical Sciences*, 2019, **152**, 346-362, doi: 10.1016/j.ijmecsci.2019.01.004.
[20] M. Sadeghi Gughari, A. R. Saidi, A. S. Rezaei, M. Askari, A. Naderi, Analytical buckling response of sectorial porous plates integrated with piezoelectric layers, *Applied Mathematical Modelling*, 2022, **101**, 811-831, doi: 10.1016/j.apm.2021.09.019.
[21] R. Madan, S. Bhowmick, Modeling of functionally graded materials to estimate effective thermo-mechanical properties, *World Journal of Engineering*, 2022, **19**, 291-301, doi: 10.1108/wje-09-2020-0445.
[22] D. Dev Singh, S. Arjula, A. Raji Reddy, Functionally graded materials manufactured by direct energy deposition: a review, *Materials Today: Proceedings*, 2021, **47**, 2450-2456, doi: 10.1016/j.matpr.2021.04.536.
[23] R. A. Ahmed, R. M. Fenjan, L. B. Hamad, N. M. Faleh, A review of effects of partial dynamic loading on dynamic response of nonlocal functionally graded material beams, *Advances in Materials Research*, 2020, **9**, 33, doi: 10.12989/AMR.2020.9.1.033.
[24] M. Hosseini, A. Jamalpoor, Analytical solution for thermomechanical vibration of double-viscoelastic nanoplate-systems made of functionally graded materials, *Journal of Thermal Stresses*, 2015, **38**, 1428-1456, doi: https://doi.org/10.1080/01495739.2015.1073986.
[25] M. Hosseini, A. Jamalpoor, A. Fath, Surface effect on the biaxial buckling and free vibration of FGM nanoplate embedded in visco-Pasternak standard linear solid-type of foundation, *Meccanica*, 2017, **52**, 1381-1396, doi: 10.1007/s11012-016-0469-0.
[26] P. R. Saffari, S. Sirimontree, C. Thongchom, T. Jearsiripongkul, P. R. Saffari, S. Keawsawasvong, Effect of uniform and nonuniform temperature distributions on sound transmission loss of double-walled porous functionally graded magneto-electro-elastic sandwich plates with subsonic external flow, *International Journal of Thermofluids*, 2023, **17**, 100311, doi: 10.1016/j.ijft.2023.100311.
[27] S. Sirimontree, C. Thongchom, P. R. Saffari, N. Refahati, P. R. Saffari, T. Jearsiripongkul, S. Keawsawasvong, Effects of thermal environment and external mean flow on sound transmission loss of sandwich functionally graded magneto-electro-elastic cylindrical nanoshell, *European Journal of Mechanics - A*, 2023, **97**, 104774, doi: 10.1016/j.euromechsol.2022.104774.
[28] C. Thongchom, P. R. Saffari, N. Refahati, P. R. Saffari, H. Pourbashash, S. Sirimontree, S. Keawsawasvong, An analytical study of sound transmission loss of functionally graded sandwich cylindrical nanoshell integrated with piezoelectric layers, *Scientific Reports*, 2022, **12**, 3048, doi: 10.1038/s41598-022-06905-1.
[29] C. Thongchom, T. Jearsiripongkul, N. Refahati, P. Roudgar Saffari, P. Roodgar Saffari, S. Sirimontree, S. Keawsawasvong, Sound transmission loss of a honeycomb sandwich cylindrical shell with functionally graded porous layers, *Buildings*, 2022, **12**, 151, doi: 10.3390/buildings12020151.
[30] N. Sundararajan, T. Prakash, M. Ganapathi, Nonlinear free flexural vibrations of functionally graded rectangular and skew plates under thermal environments, *Finite Elements in Analysis and Design*, 2005, **42**, 152-168, doi: 10.1016/j.finel.2005.06.001.
[31] V. Kumar, S. J. Singh, V. H. Saran, S. P. Harsha, Vibration characteristics of porous FGM plate with variable thickness resting on Pasternak's foundation, *European Journal of Mechanics - A*, 2021, **85**, 104124, doi: 10.1016/j.euromechsol.2020.104124.
[32] S. I. Tahir, A. Tounsi, A. Chikh, M. A. Al-Osta, S. U. Al-Dulaijan, M. M. Al-Zahrani, An integral four-variable hyperbolic HSDT for the wave propagation investigation of a ceramic-metal FGM plate with various porosity distributions resting on a viscoelastic foundation, *Waves in Random and Complex Media*, 2021, 1-24, doi: 10.1080/17455030.2021.1942310.
[33] S. K. Sah, A. Ghosh, Influence of porosity distribution on free vibration and buckling analysis of multi-directional functionally graded sandwich plates, *Composite Structures*, 2022, **279**, 114795, doi: 10.1016/j.compstruct.2021.114795.
[34] X.-L. Huang, L. Dong, G.-Z. Wei, D.-Y. Zhong, Nonlinear free and forced vibrations of porous sigmoid functionally graded plates on nonlinear elastic foundations, *Composite Structures*, 2019, **228**, 111326, doi: 10.1016/j.compstruct.2019.111326.
[35] N. L. Rosi, C. A. Mirkin, Nanostructures in biodiagnostics, *Chemical Reviews*, 2005, **105**, 1547-1562, doi: 10.1021/cr030067f.
[36] W. Xia, L. Wang, L. Yin, Nonlinear non-classical microscale beams: static bending, postbuckling and free vibration, *International Journal of Engineering Science*, 2010, **48**, 2044-2053, doi: 10.1016/j.ijengsci.2010.04.010.
[37] M. Asghari, M. T. Ahmadian, M. H. Kahrobaiyan, M. Rahaeifard, On the size-dependent behavior of functionally graded micro-beams, *Materials & Design*, 2010, **31**, 2324-2329, doi: 10.1016/j.matdes.2009.12.006.
[38] C. Thongchom, N. Refahati, P. Roodgar Saffari, P. Roudgar Saffari, M. N. Niyaraki, S. Sirimontree, S. Keawsawasvong, An experimental study on the effect of nanomaterials and fibers on the mechanical properties of polymer composites, *Buildings*, 2021, **12**, 7, doi: 10.3390/buildings12010007.
[39] N. A. Fleck, J. W. Hutchinson, A phenomenological theory for strain gradient effects in plasticity, *Journal of the Mechanics and Physics of Solids*, 1993, **41**, 1825-1857, doi: 10.1016/0022-5096(93)90072-n.

[40] F. Yang, A. C. M. Chong, D. C. C. Lam, P. Tong, Couple stress-based strain gradient theory for elasticity, International *Journal of Solids and Structures*, 2002, **39**, 2731–2743, doi: 10.1016/S0020-7683(02)00152-X.
[41] A. C. Eringen, Linear theory of nonlocal elasticity and dispersion of plane waves, *International Journal of Engineering Science*, 1972, **10**, 425–435, doi: https://doi.org/10.1016/0020-7225(72)90050-X.
[42] C. Demir, K. Mercan, H. M. Numanoglu, Ö. Civalek, Bending response of nanobeams resting on elastic foundation, *Applied and Computational Mechanics*, 2018, **4**, 105-114, doi: 10.22055/JACM.2017.22594.1137.
[43] H. M. Numanoğlu, H. Ersoy, B. Akgöz, Ö. Civalek, A new eigenvalue problem solver for thermo-mechanical vibration of Timoshenko nanobeams by an innovative nonlocal finite element method, *Mathematical Methods in the Applied Sciences*, 2022, **45**, 2592-2614, doi: 10.1002/mma.7942.
[44] C. W. Lim, G. Zhang, J. N. Reddy, A higher-order nonlocal elasticity and strain gradient theory and its applications in wave propagation, *Journal of the Mechanics and Physics of Solids*, 2015, **78**, 298–313, doi: 10.1016/j.jmps.2015.02.001.
[45] L. Li, Y. Hu, Nonlinear bending and free vibration analyses of nonlocal strain gradient beams made of functionally graded material, *International Journal of Engineering Science*, 2016, **107**, 77-97, doi: 10.1016/j.ijengsci.2016.07.011.
[46] Mohammed, Porosity and inhomogeneity effects on the buckling and vibration of double-FGM nanoplates via a quasi-3D refined theory, *Composite Structures*, 2019, **220**, 289-303, doi: 10.1016/j.compstruct.2019.03.096.
[47] M. R. Barati, A general nonlocal stress-strain gradient theory for forced vibration analysis of heterogeneous porous nanoplates, *European Journal of Mechanics - A*, 2018, **67**, 215-230, doi: 10.1016/j.euromechsol.2017.09.001.
[48] M. R. Barati, H. Shahverdi, Forced vibration of porous functionally graded nanoplates under uniform dynamic load using general nonlocal stress-strain gradient theory, *Journal of Vibration and Control*, 2018, **24**, 4700-4715, doi: 10.1177/1077546317733832.
[49] S. M. Ejabati, N. Fallah, Aerodynamic analysis of temperature-dependent FG-WCNTRC nanoplates under a moving nanoparticle using meshfree finite volume method, *Engineering Analysis with Boundary Elements*, 2022, **134**, 510-531, doi: 10.1016/j.enganabound.2021.10.021.
[50] C. H. Thai, A. M. J. Fereira, H. Nguyen-Xuan, P. T. Hung, P. Phung-Van, A nonlocal strain gradient isogeometric model for free vibration analysis of magneto-electro-elastic functionally graded nanoplates, *Composite Structures*, 2023, **316**, 117005, doi: 10.1016/j.compstruct.2023.117005.
[51] M. Rajput, A. Gupta, Strain gradient-based thermomechanical nonlinear stability behavior of geometrically imperfect porous functionally graded nanoplates, *Journal of Engineering Mechanics*, 2023, **149**, 4023040, doi: 10.1061/jenmdt.emeng-6910.
[52] Y. Jiang, L. Li, Y. Hu, A physically-based nonlocal strain gradient theory for crosslinked polymers, *International Journal of Mechanical Sciences*, 2023, **245**, 108094, doi: 10.1016/j.ijmecsci.2022.108094.
[53] S. Rebouillat, F. Pla, A review: on smart materials based on some polysaccharides; within the contextual bigger data, insiders, improvisation and said artificial intelligence trends, *Journal of Biomaterials and Nanobiotechnology*, 2019, **10**, 41-77, doi: 10.4236/jbnb.2019.102004.
[54] E. Pan, Exact solution for simply supported and multilayered magneto-electro-elastic plates, *Journal of Applied Mechanics*, 2001, **68**, 608, doi: https://doi.org/10.1115/1.1380385.
[55] N. Refahati, T. Jearsiripongkul, C. Thongchom, P. R. Saffari, P. R. Saffari, S. Keawsawasvong, Sound transmission loss of double-walled sandwich cross-ply layered magneto-electro-elastic plates under thermal environment, *Scientific Reports*, 2022, **12**, 16621, doi: 10.1038/s41598-022-20965-3.
[56] Y. Zarabimanesh, P. Roodgar Saffari, P. Roudgar Saffari, N. Refahati, Hygro-thermo-mechanical vibration of two vertically aligned single-walled boron nitride nanotubes conveying fluid, *Journal of Vibration and Control*, 2022, **28**, 2101-2120, doi: 10.1177/10775463211006512.
[57] A. Jamalpoor, A. Ahmadi-Savadkoohi, M. Hosseini, *et al*. Free vibration and biaxial buckling analysis of double magneto-electro-elastic nanoplate-systems coupled by a visco- Pasternak medium via nonlocal elasticity theory, *European Journal of Mechanics - A/Solids*, 2017, **63**, 84-98, doi: 10.1016/j.euromechsol.2016.12.002.
[58] A. Jamalpoor, A. Ahmadi-Savadkoohi, S. Hosseini-Hashemi, Free vibration and biaxial buckling analysis of magneto-electro-elastic microplate resting on visco-Pasternak substrate via modified strain gradient theory, *Smart Materials and Structures*, 2016, **25**, 105035, doi: 10.1088/0964-1726/25/10/105035.
[59] J. Y. Li, Magnetoelectroelastic multi-inclusion and inhomogeneity problems and their applications in composite materials, *International Journal of Engineering Science*, 2000, **38**, 1993-2011, doi: 10.1016/s0020-7225(00)00014-8.
[60] M. Vinyas, S. C. Kattimani, Static analysis of stepped functionally graded magneto-electro-elastic plates in thermal environment: a finite element study, *Composite Structures*, 2017, **178**, 63-86, doi: 10.1016/j.compstruct.2017.06.068.
[61] M. Vinyas, Vibration control of skew magneto-electro-elastic plates using active constrained layer damping, *Composite Structures*, 2019, **208**, 600-617, doi: 10.1016/j.compstruct.2018.10.046.
[62] Ali, Farajpour, Nonlinear frequency behaviour of magneto-electromechanical mass nanosensors using vibrating MEE nanoplates with multiple nanoparticles, *Composite Structures*, 2021, **260**, 113458, doi: 10.1016/j.compstruct.2020.113458.
[63] E. L. Sh, S. Kattimani, M. Vinyas, Nonlinear free vibration and transient responses of porous functionally graded magneto-electro-elastic plates, *Archives of Civil and Mechanical Engineering*, 2022, **22**, 1-26, doi: 10.1007/s43452-021-00357-6.
[64] M. Hosseini, M. R. Mofidi, A. Jamalpoor, M. Safi Jahanshahi, Nanoscale mass nanosensor based on the vibration analysis of embedded magneto-electro-elastic nanoplate made of FGMs via nonlocal Mindlin plate theory, *Microsystem*

Technologies, 2018, **24**, 2295-2316, doi: 10.1007/s00542-017-3654-8.
[65] B. Alizadeh Hamidi, S. A. Hosseini, H. Hayati, R. Hassannejad, Forced axial vibration of micro and nanobeam under axial harmonic moving and constant distributed forces via nonlocal strain gradient theory, *Mechanics Based Design of Structures and Machines*, 2022, **50**, 1491-1505, doi: 10.1080/15397734.2020.1744003.
[66] P. R. Saffari, M. Fakhraie, M. A. Roudbari, Nonlinear vibration of fluid conveying cantilever nanotube resting on visco-Pasternak foundation using non-local strain gradient theory, *Micro & Nano Letters*, 2020, **15**, 181-186, doi: 10.1049/mnl.2019.0420.
[67] P. Roodgar Saffari, M. Fakhraie, M. A. Roudbari, Free vibration problem of fluid-conveying double-walled boron nitride nanotubes via nonlocal strain gradient theory in thermal environment, *Mechanics Based Design of Structures and Machines*, 2022, **50**, 3665-3682, doi: 10.1080/15397734.2020.1819310.
[68] L. Li, H. Tang, Y. Hu, The effect of thickness on the mechanics of nanobeams, *International Journal of Engineering Science*, 2018, **123**, 81-91, doi: 10.1016/j.ijengsci.2017.11.021.
[69] S. F. Nikrad, A. Kanellopoulos, M. Bodaghi, Z. T. Chen, A. Pourasghar, Large deformation behavior of functionally graded porous curved beams in thermal environment, *Archive of Applied Mechanics*, 2021, **91**, 2255-2278, doi: 10.1007/s00419-021-01882-9.
[70] Y. S. Li, Buckling analysis of magnetoelectroelastic plate resting on Pasternak elastic foundation, *Mechanics Research Communications*, 2014, **56**, 104–114, doi: 10.1016/j.mechrescom.2013.12.007.
[71] L. H. Ma, L. L. Ke, J. N. Reddy, J. Yang, S. Kitipornchai, Y. S. Wang, Wave propagation characteristics in magneto-electro-elastic nanoshells using nonlocal strain gradient theory, *Composite Structures*, 2018, **199**, 10-23, doi: 10.1016/j.compstruct.2018.05.061.
[72] M. Arefi, M. Kiani, M. H. Zamani, Nonlocal strain gradient theory for the magneto-electro-elastic vibration response of a porous FG-core sandwich nanoplate with piezomagnetic face sheets resting on an elastic foundation, *Journal of Sandwich Structures & Materials*, 2020, **22**, 2157-2185, doi: 10.1177/1099636218795378.
[73] N. Kunla, T. Jearsiripongkul, S. Keawsawasvong, C. Thongchom, J. Lawongkerd, P. R. Saffari, P. R. Saffari, N. Refahati, Identification of crack location in metallic biomaterial cantilever beam subjected to moving load base on central difference approximation, *Curved and Layered Structures*, 2023, **10**, 20220196, doi: 10.1515/cls-2022-0196.
[74] C. Thongchom, P. Roodgar Saffari, P. Roudgar Saffari, N. Refahati, S. Sirimontree, S. Keawsawasvong, S. Titotto, Dynamic response of fluid-conveying hybrid smart carbon nanotubes considering slip boundary conditions under a moving nanoparticle, *Mechanics of Advanced Materials and Structures*, 2023, **30**, 2135-2148, doi: 10.1080/15376494.2022.2051101.
[75] L. Hadji, M. Avcar, Ö. Civalek, An analytical solution for the free vibration of FG nanoplates, *Journal of the Brazilian Society of Mechanical Sciences and Engineering*, 2021, **43**, 1-14, doi: 10.1007/s40430-021-03134-x.
[76] S. Ghahnavieh, S. Hosseini-Hashemi, K. Rajabi, S. Ghahnavieh, A higher-order nonlocal strain gradient mass sensor based on vibrating heterogeneous magneto-electro-elastic nanoplate via third-order shear deformation theory, *The European Physical Journal Plus*, 2018, **133**, 518, doi: 10.1140/epjp/i2018-12338-9.
[77] R. Aghababaei, J. N. Reddy, Nonlocal third-order shear deformation plate theory with application to bending and vibration of plates, *Journal of Sound and Vibration*, 2009, **326**, 277-289, doi: 10.1016/j.jsv.2009.04.044.
[78] L-L. Ke, Y-S. Wang, J. Yang, Free vibration of size-dependent magneto-electro-elastic nanoplates based on the nonlocal theory, *Acta Mechanica Sinica*, 2014, **30**, 516–525, doi: 10.1007/s10409-014-0072-3.
[79] R. Ansari, R. Gholami, Nonlocal free vibration in the pre- and post-buckled states of magneto-electro-thermo elastic rectangular nanoplates with various edge conditions, *Smart Materials and Structures*, 2016, **25**, 095033, doi: 10.1088/0964-1726/25/9/095033.
[80] C. H. Thai, A. J. M. Ferreira, P. Phung-Van, A nonlocal strain gradient isogeometric model for free vibration and bending analyses of functionally graded plates, *Composite Structures*, 2020, **251**, 112634, doi: 10.1016/j.compstruct.2020.112634.
[81] C. H. Thai, A. J. M. Ferreira, H. Nguyen-Xuan, P. Phung-Van, A size dependent meshfree model for functionally graded plates based on the nonlocal strain gradient theory, *Composite Structures*, 2021, **272**, 114169, doi: 10.1016/j.compstruct.2021.114169.
[82] A. Gupta, N. K. Jain, R. Salhotra, P. V. Joshi, Effect of crack location on vibration analysis of partially cracked isotropic and FGM micro-plate with non-uniform thickness: an analytical approach, *International Journal of Mechanical Sciences*, 2018, **145**, 410-429, doi: 10.1016/j.ijmecsci.2018.07.015.